Response of Pulmonary Artery Endothelial Cells to Altered Shear Stress Conditions

A Thesis Presented for the

Master of Science

Degree

The University of Tennessee, Knoxville

Toni Morgan Perkins

May 2025

ACKNOWLEDGEMENTS

Thank you to those who assisted me with data collection including Katarina Jones, Veronia Brown, and the University of Tennessee (UTK) Biological and Small Molecule Mass Spectrometry Core (UTBSMMSC) and the University of Tennessee Genomics Core (UTGC). Thank you to the Biomedical Engineering Department (BME) at UTK. Specifically, I would like to thank Dr. A. Colleen Crouch for the past four years of research experience, especially for keeping me a spot in her lab when I had a co-op and later transitioned into my masters. Thank you to the rest of my committee, Dr. Bryan Good, Dr. Ivis Chaple Gore, and Dr. Paul Dalhaimer for being enthusiastic and supportive of this project. I also would like to thank my undergraduate assistants, Ava Delgra and Sarah Fisher, for going on this cell culture journey with me. Finally, I would like to thank my parents for their support throughout my journey at UTK. My dad always told me I could go to any university I wanted to, as long it was UTK… and I ended up being in school for almost 6 years here! Go Vols!

PREFACE

The entirety of the cell culture space needed to be set up and cleaned prior to experimentation. This included replacing tubing in the incubator, assembling the microscope, water bath, cell counter, and dewar, and cleaning the entire room. Cell culture techniques were taught by Daniel Racz from the Chaple Lab and adjusted per lab requirements as needed. ELISA techniques were obtained from a supplier protocol and demonstrated by Desiree Denman from the Dalhaimer lab. All other techniques were sourced from literature review and colleagues. Three undergraduate students, and a SMaRT student were educated on the protocols and two undergraduate students maintain certain aspects of the cell culture lab and will continue this project.

ABSTRACT

Healthy human hearts function with two ventricles; however, single ventricle defects (SVD), a type of congenital heart defect, results in one of these ventricles not functioning properly. A series of surgeries, culminating in the Fontan procedure, are used to correct these defects, which can vary widely. The resulting Fontan physiology of the heart can cause comorbidities as the patients grow, such as pulmonary hypertension and dysrhythmias. Because this subject is understudied, it is important to determine the connection between Fontan physiology, the comorbidities, and the potential cause of the complications. It is expected that the Fontan population is to double within the next 20 years. We hypothesize that wall shear stress plays a role in pulmonary hypertension, which may be a potential cause of Fontan failure. This work aims to determine a connection between wall shear stress and expression of various molecular markers by exposing cells to various stress conditions using an orbital shaker. We found that vascular endothelial growth factor, nitric oxide, and lipids may be a potential molecular marker in clinical settings for the detection of Fontan failure.

TABLE OF CONTENTS

LIST OF TABLES

LIST OF FIGURES

CHAPTER ONE: Introduction and General Information

Congenital Heart Defects

Congenital heart defects (CHD) are one of the most common congenital malformations [1]. CHD encompasses any structural problem with the fetal heart, but one of the most severe cases is single ventricle defects (SVD) [2]. SVD is characterized by one functioning heart ventricle, rather than two (***Figure 1***). Healthy blood circulation involves the emptying of vena caval blood into the right atrium, proceeding to the right ventricle, and then to the lungs via the pulmonary arteries. After blood oxygenation in the lungs, the blood proceeds back to the left atrium via the pulmonary veins, into the left ventricle, and then the aorta. From the aorta, oxygenated blood is delivered to the body. In patients with SVD, the blood flow is abnormal through the heart, causing the mixing of oxygenated and deoxygenated blood in one single ventricle. The altered blood flow results in a lower oxygen saturation, usually below 75% [3]. The low oxygen saturation causes babies to have trouble breathing at birth, giving them a blue skin tone, deeming the term "blue babies" [4]. The low oxygen saturation can result in hypoxia induced cell damage and cell death if the SVD is not treated. CHD and SVD affect a small percentage of the United States population, and recent advances in care has increased expected survival into adulthood to approximately 90%. However, the life expectancy is still significantly lower than patients with normal heart physiology [5].

Fontan Procedure

Multiple procedures are needed to correct SVD [6]. The Fontan procedure is the last step of the reconstruction surgeries. The procedure was developed to improve quality of life for those with SVD [5]. The original Fontan procedure developed in the 1960's was a direct rerouting of the right atrium to the PA; however, many modifications have been made to improve life expectancy and quality of life [7]. The procedure was designed to bypass the right ventricle to ensure the left side has a functioning pump resulting in Fontan physiology [5], [8]. The Fontan procedure can vary greatly due to patient specific needs, which causes a wide variety in resulting Fontan physiologies. With the success of

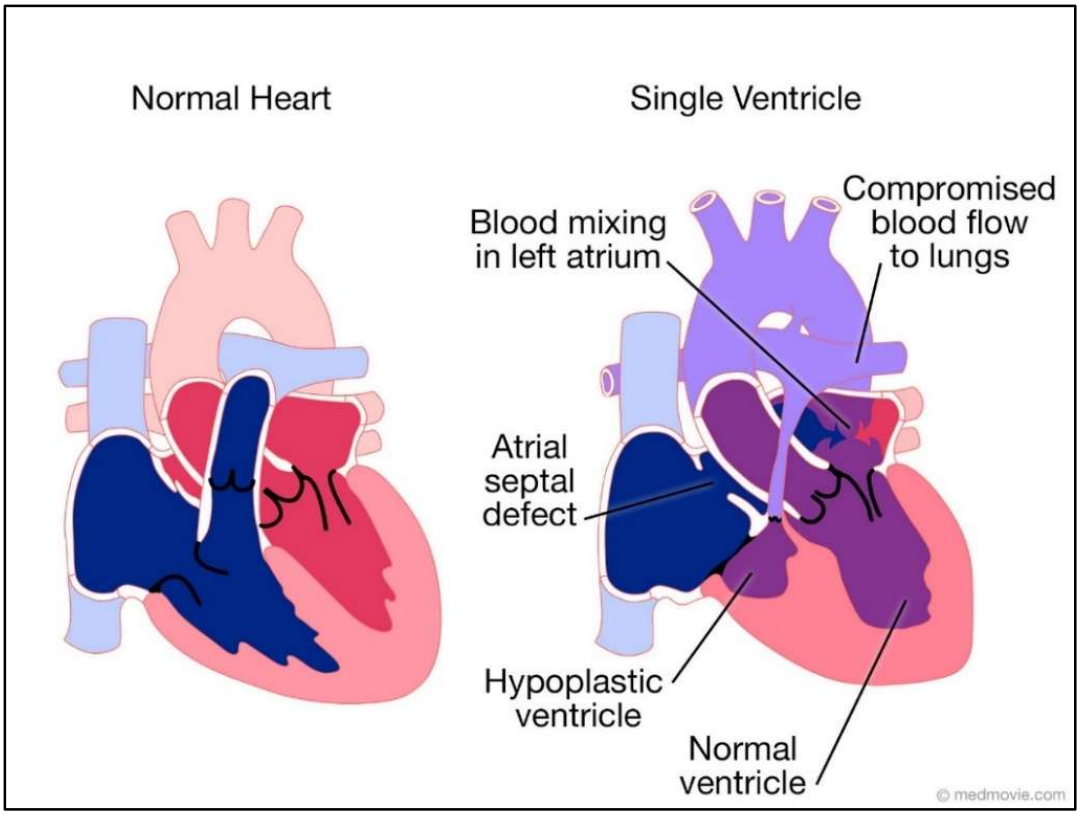

Figure 1: An Example of Normal Heart Physiology vs. SVD Physiology [9]

Fontan procedures to treat SVD, the number of adults Fontan adults is growing, but the survivors can develop comorbidities because of their changed heart physiology [9].

Fontan Failure

Although the patients are surviving through childhood and into adulthood, the procedure may lead to something known as "Fontan Failure", which results in mortality or the need for a heart transplant. This failure is a loosely applied term that characterizes Fontan Failure as exercise intolerance, reduced cardiac output, or late stages of heart failure including plastic bronchitis [9]. Out of a study of 455 adult Fontan survivors (AFS), 41% of them died, and the others required some sort of medical intervention. The majority of these AFS were young to middle aged, with a severely limited life expectancy [10]. Additionally, the number of adult patients is expected to double in the next 20 years; therefore, it is vital for researchers to understand Fontan failure and progression (***Figure 2)*** [4].

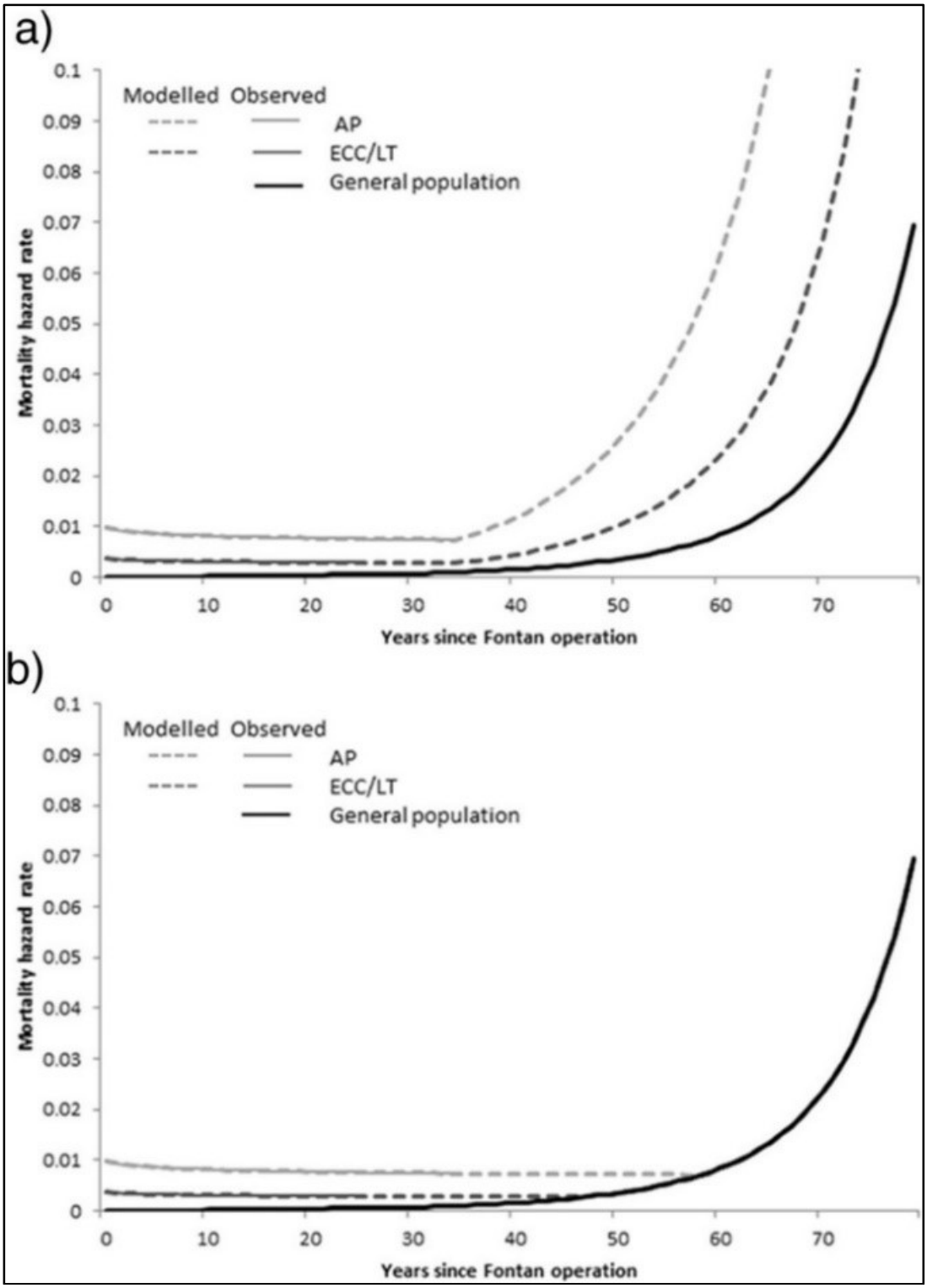

Figure 2: Mortality rates for Fontan Patients; A) Mortality projections based on constant risk, B) mortality projections based on current trends; AP = atrio-pulmonary, LT = lateral tunnel, ECC = extra-cardiac conduit [11]

Comorbidities: Pulmonary Vascular Resistance and Remodeling

Developed comorbidities may be a potential cause for Fontan Failure. Fontan patients can suffer from dysrhythmias, bronchitis, pulmonary hypertension, and hypoxemia, likely as a result from their Fontan procedure many years ago [9]. Researchers hypothesize that the developed comorbidities manifest because of the altered PA blood flow in Fontan patients. This altered blood flow through the PA may lead to increased pulmonary vascular resistance (PVR). PVR may be a large factor in Fontan failure, but PVR is not completely understood [12]. PVR is the resistance to blood flow in the pulmonary circulation and is caused by several factors. In the case of the Fontan patient, vessel diameter is constricted in response to the low oxygen levels, leading to increased resistance and causes pulmonary hypertension [13]. Pulmonary hypertension is characterized by artery pressures in excess of 25 millimeters mercury (mmHg) and often is a result of a ventricle failure and lack of oxygen. Pulmonary hypertension is accompanied by a phenomenon known as pulmonary vascular remodeling. Remodeling occurs when the arteries or veins undergo structural changes in response to micro environmental changes. The intima, composed of mostly endothelial cells (ECs), may remodel as a result of higher pressure and lack of oxygen, due to the expression of various molecular markers [14]. The entirety of the arterial walls may thicken over time and eventually progresses to complete occlusion of the arteries (***Figure 3***) [15]. The thickened walls increase PVR, potentially revealing a connection between Fontan and PVR, and pulmonary vascular remodeling [14].

Wall Shear Stress

Pulmonary vascular remodeling may be the result of endothelial cell exposure to pathological wall shear stress (WSS). WSS is generated as blood flows against the vasculature. WSS is a measurement of force over area, and the stresses are felt in the arteries, tangentially across the wall. The WSS is decreased in Fontan physiology, and the reduced shear created on the ECs causes changes in cell morphology, behavior, and signaling pathways [15]. The WSS results in the induction of several different molecular markers. For Fontan patients, molecular markers may include lipids and proteins. The

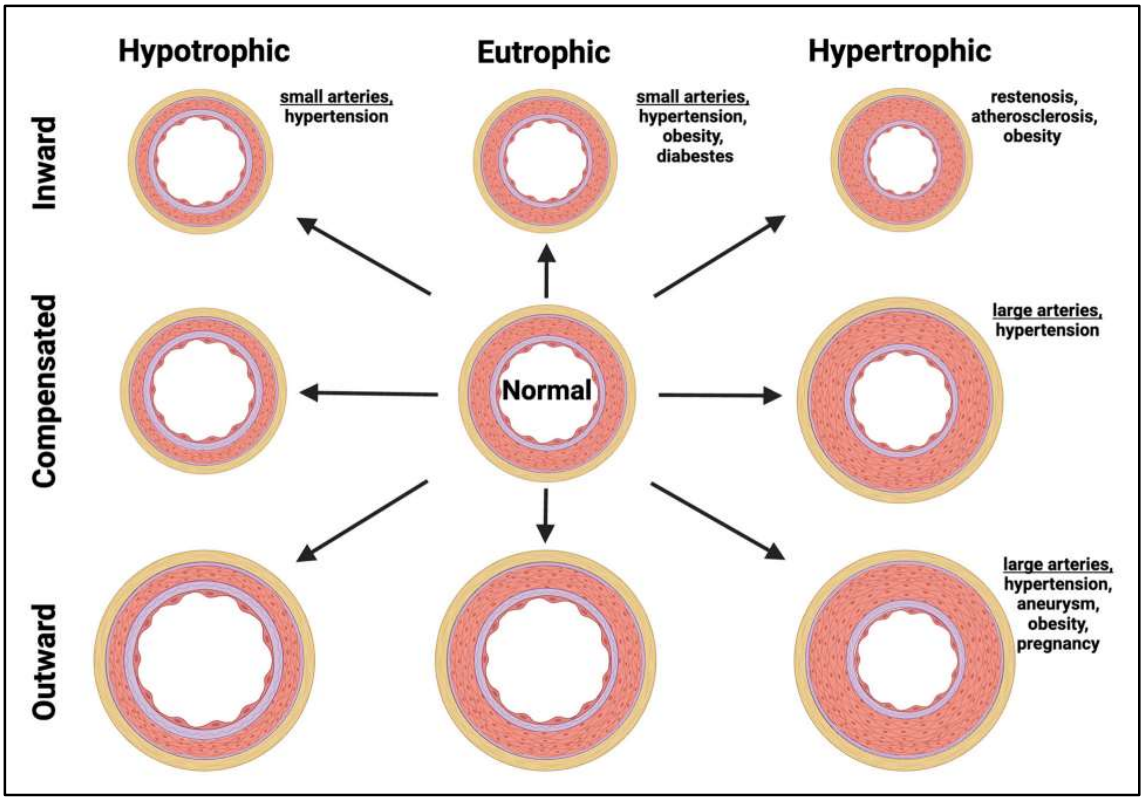

Figure 3: Variations of Pulmonary Vascular Remodeling [16]. *Fontan comorbidities may result in the hypertrophic, large artery variation of remodeling.*

induction of the markers may have connections to inflammatory responses, proliferation changes, gene expression, and other complications [17]. WSS and the induced biomarkers are hypothesized to be connected to CHD. There are over 2000 papers on this connection, yet there is a minimal amount that acknowledge the potential connection with Fontan specifically in 2024. Despite prior research, the EC response to WSS in the pulmonary artery remains widely unknown.

Research Objective

The goal of this thesis is to determine molecular marker response to altered stress conditions by subjecting human pulmonary artery endothelial cells (HPAECs) to shear stresses via orbital shaker. The molecular marker response may show insight into the potential connections between pulmonary vascular remodeling, WSS, and Fontan failure, leading to biomarker discovery and therapeutic development for SVD.

CHAPTER TWO: Literature Review

Modeling Equations

Pulmonary Vascular Resistance

The equation for pulmonary vascular resistance is related to Ohm's law, where the input pressure represents mean pulmonary artery pressure. Output pressure represents pulmonary venous pressure. Total blood flow is representative of cardiac output, as seen in (1) [18]. Poiseuille's flow is used for modeling pulmonary vascular resistance. This law relates flow to pressure, radius, length, and viscosity (2). This means small decreases in vascular radius dramatically reduces flow (***Figure 4***). Although these models are used for PVR, these are only approximations because it assumes blood flow is constant, linear, and Newtonian [19]. Physiologically, flow is pulsatile and non-Newtonian- blood becomes less viscous at high flow rates [20].

(1) $PVR = \frac{Input\ Pressure - Outpu\ \ Pressure\ (mmHg)}{Total\ Blood\ Flow\ (\frac{L}{\text{minute}})}$

(2) $Resistance = \frac{8l}{\pi r^4}$

Wall Shear Stress

The hemodynamic theory of the Poiseuille Hagen equation, which is a solution to the incompressible Navier Stokes equation (4), relates the flow rate to the vessel size. This is what was previously derived for the resistance equation (2). The pressure driving flow acts on the cross-sectional area yielding equation (5). The frictional force results in the WSS along the inner surface area of the tube (6). Finally, the shear stress equation is derived in equation (7) (***Figure 5***) [21].

(4) $\Delta P = \frac{(8Q\eta L)}{\pi r_i^4}$

(5) $F_p = A\Delta P$

(6) $F_\tau = S_\tau = 2\pi r_i L_\tau$

(7) $\tau = \frac{4Q\eta}{\pi r_i^3}$

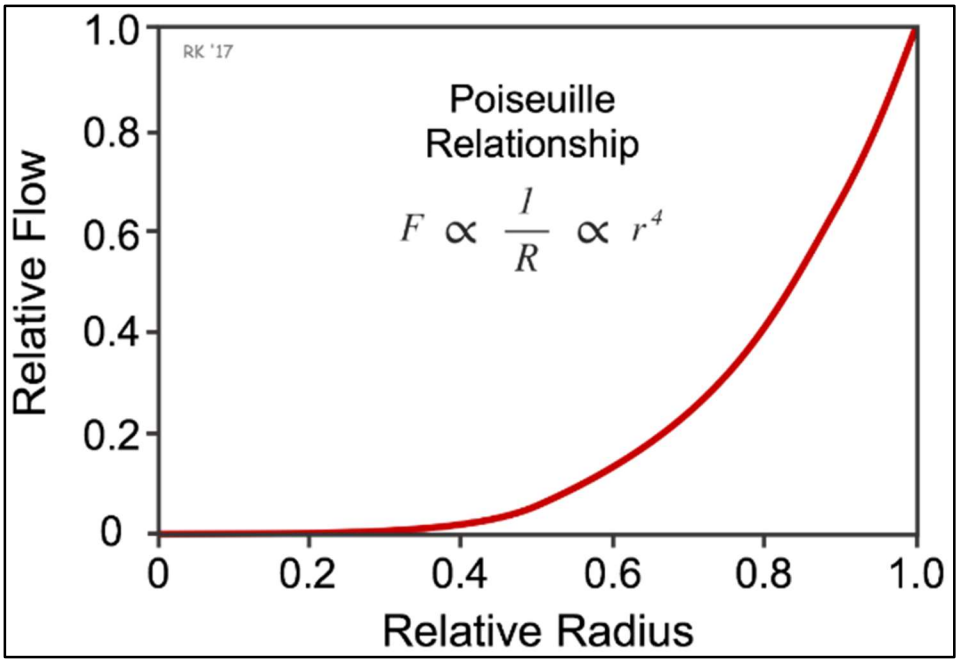

Figure 4: Poiseuille Relationship- Small decreases in vascular radius dramatically reduces flow [22].

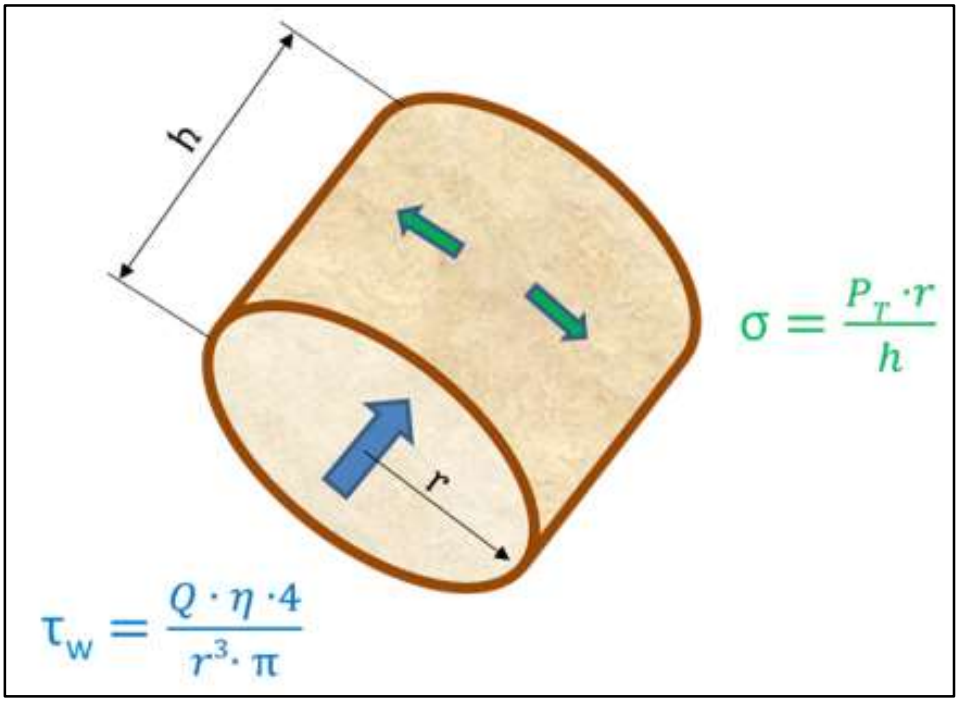

Figure 5: Hemodynamic Wall Shear Stress- Representation of vessel wall and shear stress derivation [22]

CHD and SVD Molecular Markers

Cardiovascular disease (CVD) is a group of conditions that affect structures of the heart and vascular system, and CHD falls under this umbrella. General CVD is more widely studied and therefore there is more information about potential molecular markers of cardiovascular dysfunction. Per Google Scholar search, since 2024, there are over 27,000 articles on CVD molecular markers, giving a well-rounded insight into these diseases. CHD and SVD are slightly less studied, producing an article count of 8,000 and 4,000 articles since 2024 respectively. A trend within these articles is study of the central dogma of the "omics" cascade. The cascade represents the flow of information through biological systems (***Figure 6***), and is of interest because it helps to connect the dots between predictive molecular markers and comprehensive understanding of cellular functions [23]. Genomics is outside the scope of this thesis.

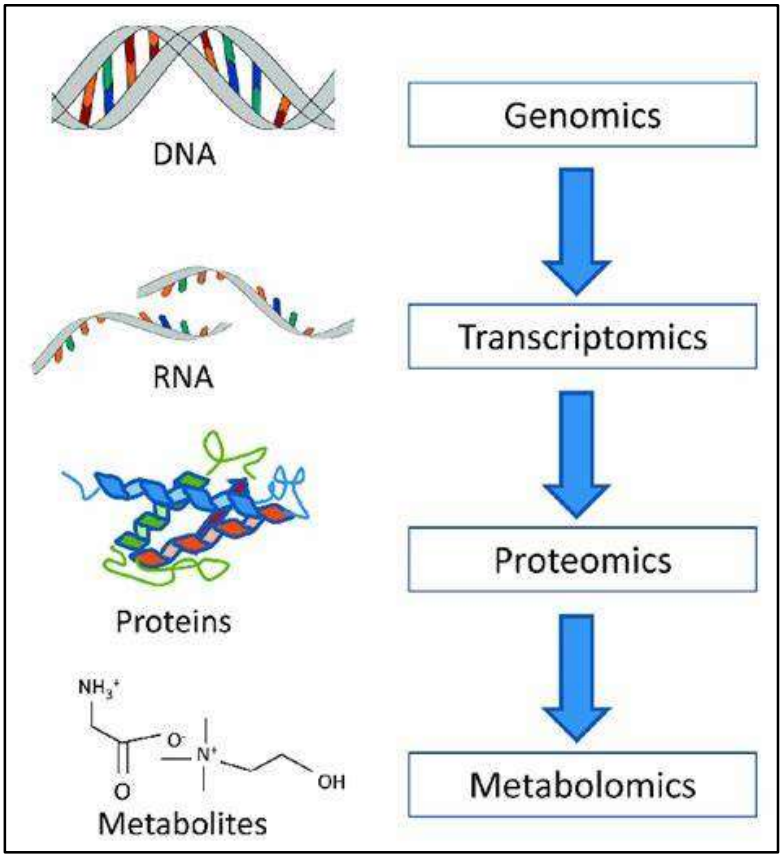

Figure 6: The Central Dogma [24]

Transcriptomics: RNA

With CVD, the cells will either up or down regulate certain genes in response. Because CVD is a large umbrella term, there are several genes that could be expressed, and may additionally be expressed in CHD. Shear stress in the heart can create an upregulation of platelet endothelial cell adhesion molecule-1 (PECAM-1). PECAM-1 mediate and regulates cardiac function and serves mainly as a communicative molecule. The fibrillin gene and TGF-Beta pathway have been found to likely be genetic and contribute to arterial remodeling. The TGF-Beta pathway is also crucial in vascular growth and inflammation [16]. Growth Differentiation Factor 15 (GDF-15) is a transforming growth factor that is expressed in the heart during oxidative stress and has been correlated with CHD. There is also N-Terminal Pro-B_type Natriuretic Peptide (NT-proBNP), a biomarker secreted in the ventricles as a response to high pressure- NT-proBNP is a well-known maker for CHD [25].

Transcriptomics: Vascular Endothelial Growth Factor

The protein, vascular endothelial growth factor (VEGF), is the main growth factor involved in proliferation and migration, and plays a role in angiogenesis. Angiogenesis is induced by hypoxia and increased shear stress. VEGF is well studied in the heart and considered a biomarker for CVD. High levels of VEGF are normal in a healthy heart. When the heart function is not optimal, a VEGF change is suspected to occur [26]. In an attempt to maintain homeostasis, overtime the cells may overproduce VEGF [27]. VEGF is a vital contributor to the survival of fetuses developing CHD. Feucht et al. found that VEGF is required for proper vascular development, and a severe lack of VEGF can potentially cause CHD [28].

Metabolomics: Nitric Oxide

Nitric oxide (NO) is produced by the endothelial nitric oxide synthase (eNOS) and plays a crucial role in preventing cardiovascular disease. VEGF is induced by NO and connects to eNOS receptors due to hypoxia. NO serves as a vasorelaxant that prevents the proliferation of smooth muscle cells [29]. With CVD, endothelial cell function is altered, reducing the expression of NO, creating a wide range of effects [30]. The downregulation of eNOS is a result of the hypoxic microenvironment from the SVD

patient's physiology. NO is also decreased in infants with CHD. Sometimes, this lack of NO in the body is treated with inhaled NO [31]. The inhaled NO has demonstrated to decrease arterial pressure and increase oxygen saturation [32].

Metabolomics: Lipids

A key molecular marker for CVD are lipids, of particular note-phosphatidylethanolamine (PE) and triglyceride (TG). HPAEC membranes are mostly composed of PE lipids, which are also found in the mitochondrion [33]. PE lipids have varying functions, but generally are related to membrane topology and oxidative phosphorylation [34]. TG lipids are found in the fat deposits of mammals and are one of the greatest indications of CVD when levels are elevated [35]. Lipidomics in infants with CHD reveals that PE, phosphatidylcholine (PC) and phosphatidylinositol (PI) were detected as important lipid classifications [36].

Role of Shear Stress in Fontan

Transcriptomics: RNA

Fontan patients also have a distinct gene transcriptome, and there are expression distinctions between pre operative and post operative samples [37]. for example, Protein Delta Homolog 1 (DLK-1), an angiogenesis starting epidermal growth factor, was found to be over expressed in surviving Fontan patients. On the other hand, there is Suppression of Tumorigenicity 2 (ST2), an interleukin receptor that is a marker for remodeling, apoptosis, and heart failure. There is also von Willebrand Factor (vWF), an endothelial cell produced mediator of inflammation. Increased levels of vWF have shown an increase risk of heart failure, especially in Fontan patients [25].

Transcriptomics: Vascular Endothelial Growth Factor

Fontan molecular markers also include VEGF, and the molecular response is similar to CHD. Cells may release VEGF in response to injury, which in turn induces proliferation of the cells. In a study by Evans et al, pulmonary hypertension correlated with an increase in VEGF production [38]. This suggests that at higher laminar shear, and lower complex shear, there will be higher concentrations of VEGF. Saraf et al. found similar respective concentrations of VEGF and showed the VEGF levels increased with worsening Fontan failure [39].

Metabolomics: Nitric Oxide

In the Fontan physiology, eNOS is decreased, and therefore NO production is limited [40]. There is evidence that pulmonary hypertension induced endothelial dysfunction could be caused by decreased NO production [41]. NO also has connections between increased proliferation and remodeling due to its ability to induce VEGF production [14], [29].

Metabolomics: Lipids

Lipids play an important role in signaling pathways and metabolic regulation. In the context of shear stress in Fontan patients, literature review has shown potential lipids are PE, PC, and (sphingomyelin) SM, which makes them of interest as potential biomarkers for Fontan Failure [42]. In a study in 2020, blood samples were collected from Fontan patients and a metabolomic examination was completed. Michel et al. found that these lipids were significantly under expressed in comparison to a healthy person. A potential cause for this is the decrease in shear stress in the Fontan system, which has been shown to alter cell signaling pathways [42].

Research Gap

The gap in this research arises as the largest population of Fontan patients enters adulthood. In the past, there has been a limited number of patients who underwent the procedure, however, that population is growing now, and can be studied to potentially prevent Fontan failure (***Figure 7***) [43]. The research completed in this thesis entails applying shear stresses to a culture of primary endothelial cells, with the goal of determining a connection between molecular markers and WSS. The molecular markers may give insight into a connection between WSS, pulmonary avascular resistance, and Fontan Failure.

Methodology Justification

Cell Culture Techniques

Cell culture techniques vary widely, and there are several methods to seeding, culturing, and passaging cells. Booyse et al., in 1975, utilized bovine arterial endothelial cells over a series of 14 months to determine their viability over time. Cells were grown in a Hepes buffer and FBD, then cultured to 90% confluency. Subculture passaging was

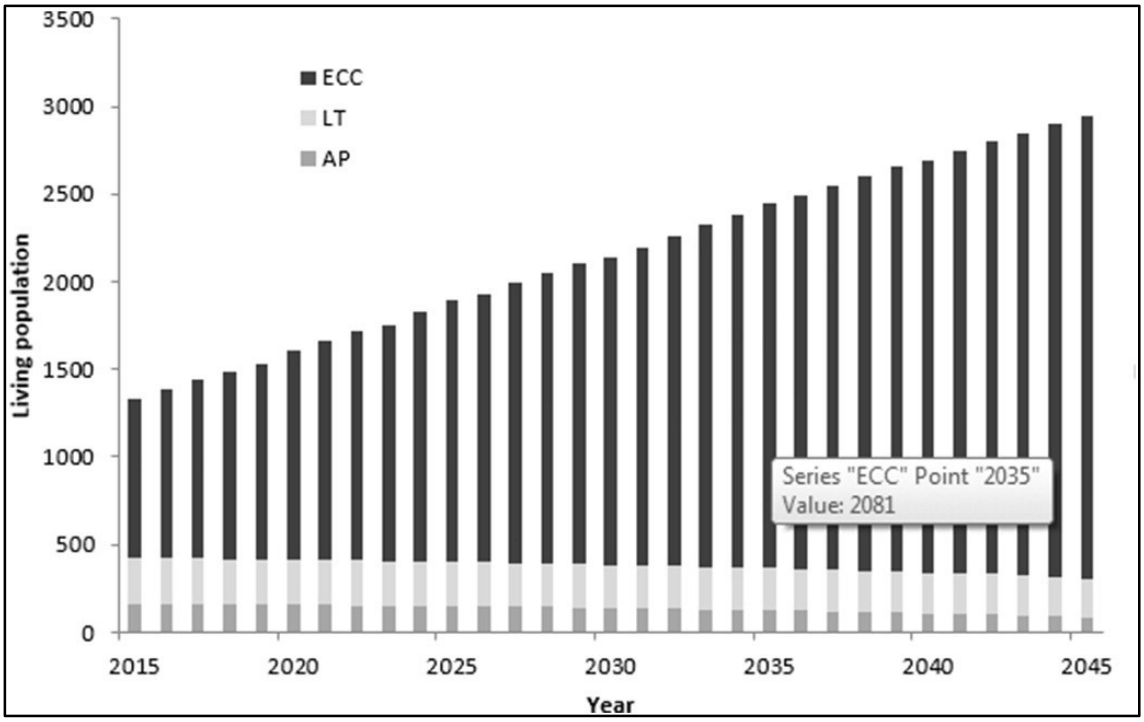

Figure 7: Growing Fontan Survivor Population [11]

performed with trypsin-EDTA over 35 passages. It was discovered that this methodology did not cause any apparent change in morphology [44]. Even though this paper was written in 1975, these techniques are still used. For example, in a 2003 article by Chatterjee et al., bovine vascular endothelial cells were cultured in Dulbecco's modified Eagle's Medium, FBS, and penicillin/streptomycin [45]. Although these cells were sourced from bovine, human cells require similar media and care. A study similar to this thesis used human umbilical vein endothelial cells (HUVECs) to determine the induction of genes from shear stress. In that study, the authors used medium, FBS, heparin, endothelial cell growth supplement (ECGS), and penicillin/streptomycin [46]. This general methodology serves as the basis for the cell culture in this work. After experimentation, cells need to be removed from the flask for subculturing or collection. This is because the cells are adherent and require assistance either enzymatically or mechanically to detach. A common method of this is utilizing trypsin EDTA, tapping, or scraping of the cells. Trypsin EDTA is a combination of the digestive enzyme trypsin, and

EDTA which is a chelating agent. It aids in detaching cells by weakening peptide bonds. There has been speculation that this mixture causes a change in results of testing, however in a study by Hemming, et. Al, the authors found that there was no effect [47]. In some cases, the trypsin EDTA does not completely detach the cells, or the researcher desires a method with no chemicals. This method would involve mechanically tapping or scraping the cells from the flask. Utilizing both methods would result in the highest quality of detached cells for further subculturing or collection. Subculturing involves "splitting" the quantity of cells between a few flasks to allow for proliferation. A traditional method of this is to split the cells from 1 to 3 flasks because the population doubling rate for HPAECs is approximately upwards of 4 days [48]. On the other hand, for collection, the methodology depends on the requirements of the testing.

Applying Shear Stresses

Dekker et al. used ta parallel plate-type flow chamber to apply shear stresses [46]. This technique for applying shear stress is one of the most common methods used *in vitro*. It is simple in design, and the stresses are well defined due to the geometry of the chambers [49]. Another method of applying shear stresses, is that of the cone and plate. Franzoni et al, developed a cone and plate geometry that was used to deliver stresses. The authors found that the device applied uniform stresses and that the flow conditions could be reproduced [50]. Cone and plate geometries are also quite common and used in shear stress research [51]. Another method for applying shear stress on the cells is the use of an orbital shaker. An orbital shaker is a device that is used to induce shear stress via circular movement on platform. A study completed by Hyosoo et. al, showed that the orbital shear stress created by the shaker, is not a consistent shear force. This is because the inner and outer portions of the experimental wells, show different results [52]. However, this is not necessarily a downside to this method, while the outer wall of the well may experience laminar flow similar to that of normal physiological conditions, the center experiences a low shear stress which is characteristic of the Fontan physiology [53]. The availability and ease of use of these orbital shakers also demonstrate its advantages.

Detection of Molecular Markers

Messenger ribonucleic acid (mRNA) sequencing can measure gene expression and often provides a more complete picture than DNA sequencing because RNA transcription plays a critical role in cell growth and development. There are different variations, however the most widely used technology is bulk sequencing; it reveals the average gene expression to understand molecular mechanisms [54]. It works by isolating the RNA, selecting or depleting the RNA, and then synthesizing cDNA to form a library. Enzyme linked immunosorbent assays (ELISA) are a common laboratory technique that detects various biomarkers from fluid samples. It works by quantifying an antigen and allowing it to bind with an antibody. Unbound antibodies are washed away after an enzyme substrate is added [55]. During this test, a visible color change takes place, which can be interpreted both qualitatively and quantitatively by absorbance. There are different variations of ELISA. For biomarkers in HPAECs, the indirect sandwich ELISA proves to be the best option, as it is highly sensitive, highly specific, and flexible with discrepancies. This ELISA uses a coated plate to determine total concentration of biomarkers in complex samples [56]. Liquid chromatography-mass spectrometry (LCMS) is an analytical technique used to analyze metabolites and lipids from biological samples. There are varying techniques when preparing and processing samples. For example, hydrophilic interaction chromatography (HILIC) analysis aids in solid-phase extraction, the preferred method for cell samples. The samples are passed through a column that responds to light absorption, resulting in an intensity peak. The mass spectrometer then completes a mass-based detection of the compounds- the molecules are ionized, and separated by mass-to-charge ratios [57].

Collagen Co-Cultures

The previous techniques and studies used HPAECs in a monolayer of cells; these methods are insightful for internal cell signaling, however key aspects of the external microenvironment are neglected. To fully understand the mechanisms, collagen co-cultures can be used to model the structural elements of the pulmonary artery. Collagen I, is the most abundant type of collagen in the human body, and serves as a structural component for blood vessels [58], [59]. Using collagen gels demonstrates cell migration,

signaling between cell types, and allows for spatial analysis of biomarkers. Constructing the collagen gels proves to be a difficult task despite having the same general preparation method across disciplines. In a study by Ziegler et al, the authors utilize a methodology originating from the 1970s- it involves diluting the collagen with NaOH, FBS, and cell culture media to prepare a gel. The endothelial cells were then seeded onto the collagen gel as the cells would have been onto a flask with no collagen [60]. A study completed in 2016 used a similar preparation method, demonstrating that, although difficult, the method is the gold standard for preparing collagen gels for a co-culture [59].

CHAPTER THREE: Methodology

Materials

*A methodology workflow can be see*n *in* ***Figure 8*** *and full table of materials is provided in* ***Table 1.***

1D Cell Culture

Primary human pulmonary artery endothelial cells (HPAEC) were cultured in endothelial cell growth medium. The culture was supplemented with 0.02 mL/mL fetal calf serum (FCS-10), 0.004 mL/mL endothelial cell growth supplement (ECGS/H), 0.1 ng/mL epidermal growth factor (hEGF-0.05), 1 ng/mL basic fibroblast growth factor (hbFGF-0.5), and 1 µg/mL hydrocortisone (HC) for growth and culture. For experimental purposes, the media consisted of only 0.02 mL/mL FCS-10 to avoid assay signaling. The cells were thawed in a water bath at 37 degrees Celsius (°C) and seeded at 10,000 cm^2 into T75 culture flasks to maximize cell growth prior to subculturing. The cells were then incubated at 37°C and 5% carbon dioxide (CO_2) in an Isotemp incubator. For passaging, 0.05% trypsin-EDTA and mechanical tapping were used to induce cell detachment from the flasks. All unused cells were distributed between cryovials and pelleted in cryopreservation media, then placed in a slow cooler in a -80˚C freezer for 24 hours. The cryovials were then transferred to a liquid nitrogen dewar until testing. Testing was done at passages between passages 4-8 in 12-well plates, and specific experimental groups can be seen in ***Table 2.*** Certificates of analysis for the HPAECs can be found in the appendix on page 77.

Computational Fluid Dynamics

A series of computational fluid dynamics simulations were completed to validate the experiment. The simulations were completed by committee member, Dr. Bryan Good, in which he used Open Foam to simulate the shear stresses in the 12-well plates from the orbital shaker. Good utilized the programming to collect average, maximum, and minimum stress values. In addition, graphics interchange formats and still images were collected from these simulations. The following equations were used in the analysis of the orbital shaker motion:

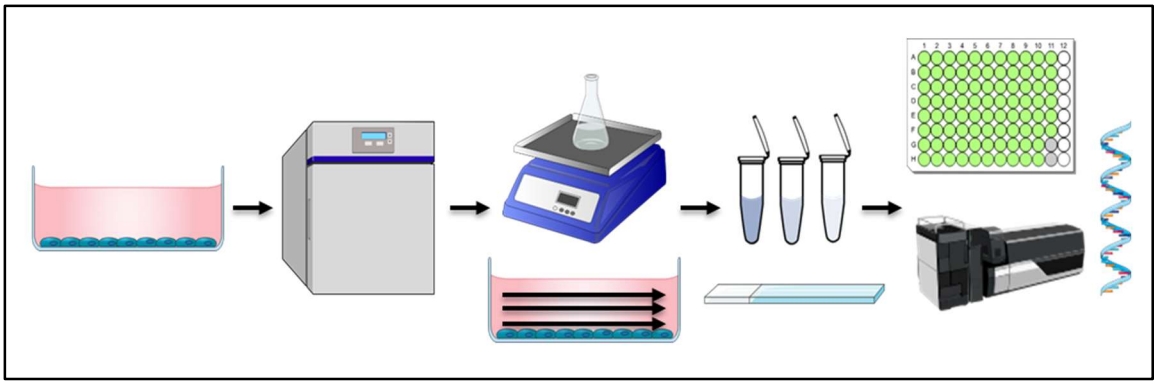

Figure 8: Methodology Work Flow- Cell culture, incubation, application of shear stresses via orbital shaker, collection of samples via spotting and Eppendorf tube, testing via ELISA, LC-MS, and Bulk RNA

Table 1: List of Materials including amounts needed for 12-well plates, the source, and part number

Material	**Amount for 12 Well Plate**	**Source**	**Part Number**
HPAEC	100,000 cells	PromoCell	501Z019.10
Cell Media	1 mL/well	PromoCell	C-22210
FBS	5%	Gibco	C-39210
Trypsin	1 mL/well	Gibco	25200072
PBS	2 mL/well	Gibco	10010031
CryoSFM	2 mL/vial	PromoCell	C-29920
Trypan Blue	20 µl	Gibco	15250061
Cryovials	12 vials/plate	Thermo Scientific	UX-06754-96
VEGF ELISA	1 kit	Sigma Aldrich	RAB0508-1KT
NO ELISA	1 kit	Sigma Aldrich	MAK454-1KT
Bulk mRNA	1 kit	QIAGEN	-
Incubator	N/a	Thermo Scientific	-
Centrifuge	N/a	Thermo Scientific	-
Water Bath	N/a	Thermo Scientific	-
Cell Counter	N/a	Invitrogen	-
Microscope	N/a	VWR	-
Biosafety Cabinet	N/a	Thermo Scientific	-
Pipets	Several	VWR	varying
Mr. Frosty	1	Thermo Scientific	5100-0001

Table 2: Final Experimental Groups and Naming Convention

	Supernatant	**Cells**
	1S	1C
	2S	2C
	3S	3C
	4S	4C
0 RPM	5S	5C
	6S	6C
	7S	7C
	8S	8C
	9S	9C
25 RPM	10S	10C
	11S	11C
	12S	12C
	13S	13C
	14S	14C
50 RPM	15S	15C
	16S	16C
	17S	17C
	18S	18C
	19S	19C
75 RPM	20S	20C
	21S	21C
	22S	22C
	23S	23C
100	24S	24C
RPM	25S	25C

(8) $TAWSS = \frac{1}{T}\int_0^T WSS \cdot dt$

(9) $OSI = \frac{1}{2}(1 - \frac{\left|\frac{1}{T}\int_0^T WSS \cdot dt\right|}{\frac{1}{T}\int_0^T |WSS| \cdot dt})$

Where TAWSS is time averaged wall shear stress, and OSI is oscillatory shear index. Forces in the x and y directions can be calculated with angular velocity in radians per second, shaking diameter in meters, and time point in seconds [61].

Shear Stress Application

For the WSS experiment, cells were passaged and seeded on 12-well plates at ~100,000 cells/cm^2 and allowed to achieve 90% confluency prior to experimentation. Experimental groups were determined (***Table 2***) and replicated three times at 0 rotations per minute (RPM), 25 RPM, 50 RPM, 75 RPM, and 100 RPM. The remaining supernatant from the wells were aliquoted in tubes in volumes of 1 mL for each experimental group. The cells were then trypsinized, stained using trypan blue, and then counted with a Countess cell counter in replicates of 3. After the experiment, the cells were trypsinized, stained using trypan blue, and then counted once again. 2 µl of cell suspension was spotted onto glass slides, for future potential Mass Spectrometry Imaging (MSI). The remaining cellular samples were separated in tubes in volumes of 1 mL of cell suspension for each experimental group. These slides and tubes were stored at -80˚C until testing.

Bulk mRNA

The bulk mRNA protocols were followed as provided in the kit from the provider (QIAGEN). RNA library preparation was completed by the University of Tennessee Genomics Core (UTGC).

Vascular Endothelial Growth Factor and Nitric Oxide ELISA

The ELISA protocols were followed as provided in the kit from the provider (Sigma Aldrich). This documentation can be found in the appendix on pages 64 and 68. After the protocol, the plates were put into a microplate reader and read at the specific absorbance needed.

LC-MS

Lipid extractions and mass analyses were performed at the Biological and Small Molecule Mass Spectrometry Core (BSMMSC) at the University of Tennessee Knoxville (RRID: SCR_021368). Benchtop total lipid extractions were performed on 40µL of sample using a modified version of the Bligh and Dyer extraction protocol. Briefly, 750µL of 1:2 chloroform:methanol, 250µL of chloroform, and 250µL of water were added to each sample. Samples were vortex and centrifuged for 10 minutes at 17,000 x g. The lower organic phase was collected and the aqueous layer re-extracted with 250µL chloroform. The combined organic layers were dried under a steady stream of nitrogen and resuspended in 150µL 9:1 methanol:chloroform and stored at 4 ºC prior to mass analysis.

Polar lipids were separated and analyzed using hydrophilic interaction chromatography (HILIC) coupled to a high-resolution mass spectrometer (HRMS). The chromatographic separations were performed as previously described. All solvents used were LCMS grade (Fisher Scientific). The separations were performed using an UltiMate 3000 UHPLC system (Dionex). Mobile phase A consisted of 10mM ammonium acetate in 50:50 acetonitrile:water (pH8) and mobile phase B consisted of 10mM ammonium acetate in 95:5 acetonitrile:water (pH8). The separations utilized an Acquity BEH HILIC column (1.7µm, 2.1 x 100mm; Waters) with a 10-minute linear gradient from 100% to 80% mobile phase B and one minute equilibration at 100% mobile phase B. The flow rate was set to 0.5mL/min throughout the separation. The eluent was introduced to a Q Exactive Plus orbitrap mass spectrometer (Thermo Scientific) via electrospray ionization (ESI). For a more comprehensive analysis, each sample was analyzed with both positive and negative polarity modes. Ionization parameters were as follows: spray voltage was set to 3.3kV, capillary temperature of 350°C, sheath, aux, and sweep gases were set to 25, 10, and 0 arbitrary units, respectively, and S-lens RF level was set to 50. Mass analysis was performed using data dependent acquisition. The scan range was 100-1500 m/z with a resolution of 140,000 and AGC target of 3e6. The fragmentation scans used a stepped collision energy of 15, 30, and 45 eV with 35,000 resolution, AGC target of 1e5, and dynamic exclusion of 10s.

Water soluble metabolites were also extracted and analyzed at the BSMMSC. Extractions were performed at 4ºC using an established protocol. An aliquot of each sample (40µL) was mixed with 1.3mL of extraction solvent (4:4:2 acetonitrile:methanol:water with 0.1 M formic acid. The mixture was left at - 20ºC for 20 minutes prior to centrifuging at 17,000 x g for 5 minutes. The supernatant was collected and the pellet was re-extracted with 200µL extraction solvent. The combined supernatant was dried under a steady stream of nitrogen and resuspended in 200µL of water and stored at 4 ºC prior to mass analysis.

Metabolomics samples were separated using a previously validated UHPLC-HRMS method. The 25 minute separations were carried out using a Synergi Hydro-RP column (2.6µm, 100 mm x 2.1 mm, 100 Å; Phenomenex) with an UltiMate 3000 UHPLC system (Dionex). Mobile phases consisted of 97:3 water: methanol with 11mM tributylamine and 15 mM acetic acid (A) and 100% methanol (B). All solvents used were LCMS grade (Fisher Scientific). The eluent was introduced to an Exactive Plus Orbitrap Mass Spectrometer via electrospray ionization with negative polarity. The mass spectral analysis was performed as described previously.

Data Analysis

ImageJ was used to set the scale, measure length, and width of the cells. An average of the measurements was taken from multiple cells using the built-in measurement tools. Excel was used for basic calculations including percent fold change noted in (12). JMP was used for numerical data analysis. A one-way analysis of variance (ANOVA) was run on the data sets and used to produce the figures seen throughout the thesis. Also, in JMP, the non parametric tests, Kruskal Wallis and Dunn, were run to establish statistical significance. Standard errors are shown instead of standard deviations because of the small biological sample size. The standard error shows the precision rather than the deviation from the mean [62].

(12) $fold\ change = \frac{final}{final}$

Literature Review

Literature review was completed with Google Scholar, UTK Libraries, and Zotero annotation for citation generation.

Development of 2D Cell Culture

Attempt of the collagen gel was completed with rat tail collagen. The collagen was neutralized using ammonium hydroxide, cell culture media, and PBS as listed in the appendix on page 75 and deposited into 12-well plates to set into a gel.

CHAPTER FOUR: Results and Discussion

Preliminary Shear Results

Preliminary testing was conducted with HPAECs under shear stresses for a grant submission using T25 flasks as the culture vessel. The geometry of the T25 flasks was not ideal, as their surface area consumed materials at a high rate and cells took longer to reach confluency in a T25 flask- 2,800,000,000 cells. Additionally, the geometry was inconsistent with the goals for the project; T25 flasks are rectangular in shape, and corners created irregular stresses. To eliminate these concerns, 6-well, and 12-well plates were used for the next experiments. HPAECs were subjected to shear stresses at 15, 115, and 215 RPM for 0-72 hours at passages 4-6. Experimental groups can be seen in ***Table 3***.

Cell Counts

Cell count was lower at low RPM but increased toward 115 RPM. However, at 215 RPM, the cell count dropped (***Figure 9***), ***(Table 4)***. Although there was no statistical difference between the RPM groups likely due to large variation, the trends in data are discussed. It is expected at higher RPM to have higher cell counts due to shear induced proliferation, the results at 215 RPM may likely be connected to cell signaling pathways being severely disrupted. Another potential cause for the low count at 215 may be the magnitude of the stresses being too high and shearing the cells from the flask. There is also evidence that the increased shear also reduces cell viability and increases apoptosis rates via the Akt phosphorylation pathway [63]. The Akt phosphorylation pathway was found in another study to mediate the activation of eNOS, leading to increased NO production in higher shear stresses [64]. Because the cell counts decreased, this led to the choice to lower the range of RPM slightly to allow for cell proliferation and viability to lower the risk of cells hearing off of the flasks. Realistically, higher RPM represents healthy shear as found in the human body and would be approximately 1.4 Pa or 0.14 dyne/cm^2 [65]. Therefore, lower RPM would be more representative of Fontan physiology.

Table 3: Preliminary Experimental Groups and Naming Convention. No names were noted for stationary 115 RPM because this experiment was completed quickly.

		Time (Hours)			
		72	**48**	**24**	**0**
RPM	**15**	A1	B1	C1	D1
		A2	B2	C2	D2
		A3	B3	C3	D3
	115	X1	Y1	Z1	-
		X2	Y2	Z2	-
	215	E1	F1	G1	H1
		E2	F2	G2	H2
		E3	F3	G3	H3

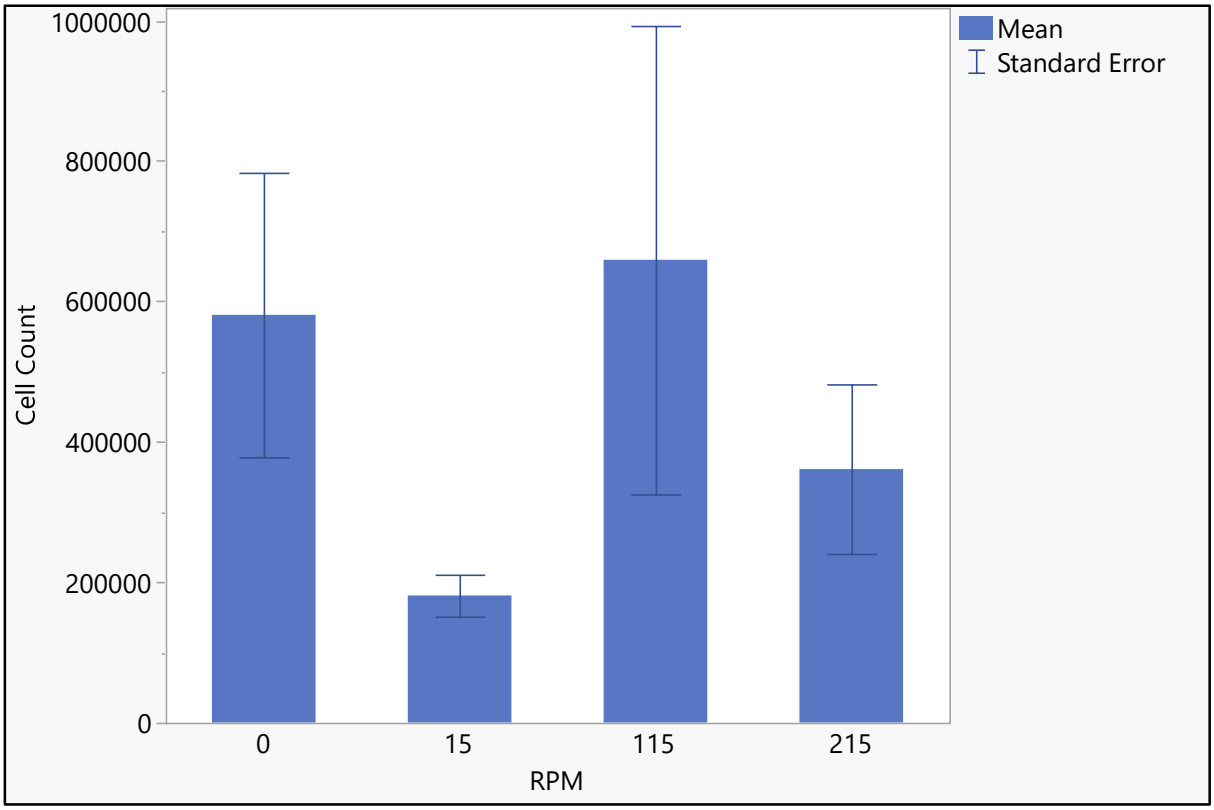

Figure 9: Preliminary Experiment- Final Cell Counts; 0, 15, 115, 215 RPM. No statistical differences. Highest final cell count was at 115 RPM, and lowest at 15 PRM.

Table 4: Preliminary Experiment- Final Cell Counts; No values were noted for stationary 115 RPM because this experiment was completed quickly.

		Time (Hours)			
		72	**48**	**24**	**0**
RPM	**15**	125,700	188,400	188,400	62,700
		1,005,000	78,600	228,600	266,700
		94,200	738,000	125,700	188,400
	115	1,884,000	519,000	750,000	-
		125,700	15,690	31,500	-
	215	219,600	705,000	534,000	690,000
		298,200	690,000	549,000	942,000
		172,500	801,000	330,000	1,335,000

Metabolomics: Lipids

LCMS was completed on both cells in positive and negative mode for preliminary lipidomics in the endothelial cells. The preliminary lipid profiles revealed that PI 34:2|PI 16, SM 12, PI 39, and PE 38:4 were some of the highest expressed lipids after being subjected to 24 hours of 115 RPM. All these lipid species have been implicated in CVD, including the comorbidities of the Fontan procedure. PI lipids play a large role in signaling pathways, specifically apoptosis, SM lipids are connected to signaling as well, and PE lipids maintain the cellular membranes. In regard to their roles in the heart, PI lipids have been show to increase and remodel cells due to increased work [66]. Both SM and PE lipids have been linked to vasoconstriction and hypoxia [36], [67]. Of particular note, PE 38:4 has been linked to hypertension in CVD and may play a potential role in remodeling [68], [69]. Additional significant lipid species and their corresponding cardiovascular relationship are listed in ***Table 5***, the most prominent correlation being between PC lipids and CVD disease mortality.

Experiment 1

Further developing the research plan, there was a switch to 6-well plates to minimize overconsumption of materials, as well as to match the circular motion of the orbital shaker. RPM was set to 50, 100, and 200 RPM because there was no statistical difference and at 215 RPM, the cells were thought to be losing function. The time frame

Table 5: Experiment 1- Significant Lipids;

Lipid	p Value	Relationship
PI 36:1	0.0035	Atherosclerosis, cardiac death [70]
PC 38:6	0.0211	Cardiovascular disease mortality, hypertension [71]
PE 34:2	0.0241	Cardiovascular disease [68]
PC 32:2	0.0321	Cardiovascular disease mortality [71]
PC 34:2	0.0377	Cardiovascular disease mortality [71]
PC 32:1	0.0408	Hypertension [69]
PC 30:1	0.0497	Cardiovascular disease mortality [71]

was reduced from 72 hours to 24 hours because there was no statistical difference found over an extended period. The addition of varying passages was to determine if the age of the cells had any impact on their biomarker expression. The experimental groups for experiment 1 are shown in ***Table 6.***

Computational Fluid Dynamics

The computational fluid dynamics for experiment 1 are not as refined as those for the final experiment. The CFD for this experiment required the addition of more accurate fluid density and viscosity, mesh refinement, and longer run-time to ensure steady-state stresses. However, the CFD did reveal some key points to consider for the results of experiment 1. In ***Figure 10*** **B)** and **C)**, there is a distinct line of higher magnitude stress. This was revealed to be the "line" of the cell culture media sloshing in the well plate. The cells encountered a higher magnitude of stress when the cell culture media would first spin around the plate. Especially in the 200 RPM case, the stress pattern follows the cell culture media exposing the cells to air. The CFD for the 200 RPM case showed that the cell culture media did not completely cover the well plate, instead left certain areas exposed. This exposure was confirmed by dying the media to reveal open space on the well plate. Because of this, the results for the 200 RPM case may be affected, as the cells must be covered by cell culture media at all times to survive. This exposure to air may be representative of hypoxic conditions because cell culture media acts as the delivery mechanism of oxygen to the cells. These CFD simulations also revealed that 200 RPM is representative of healthy human physiology.

Table 6: Experiment 1 Groups and Naming Convention

		Passage		
		4	**6**	**12**
RPM	**0**	A1	B1	C1
		A2	B2	C2
		A3	B3	C3
	50	D1	E1	F1
		D2	E2	F2
		D3	E3	F3
	100	G1	H1	I1
		G2	H2	I2
		G3	H3	I3
	200	J1	K1	L1
		J2	K2	L2
		J3	K3	L3

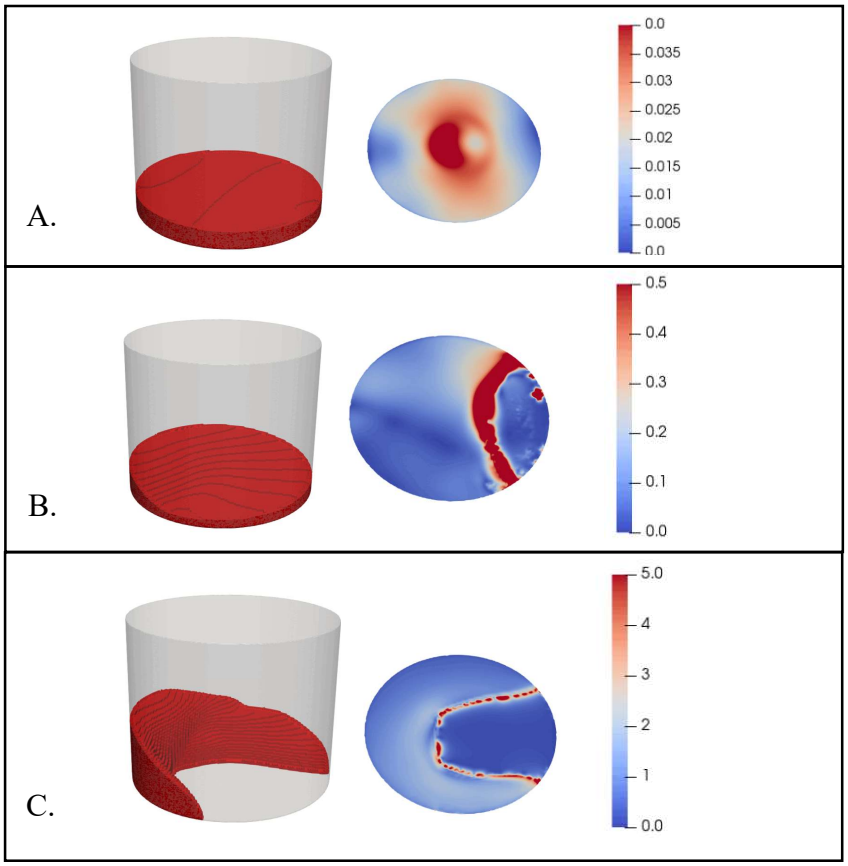

Figure 10: Experiment 1- Wall Shear Stress Simulations; Demonstrate example of fluid motion in the well plate. Values seen in figure are not directly correlated to the same time points. A) 50 RPM, B) 100 RPM, C) 200 RPM. Scale is in Pascals (Pa).

Cell Counts and Viability

With higher RPM there was more cell proliferation, but less viability compared to the lower RPM which has less proliferation and more cell viability. This aligns with preliminary testing, as well as literature review that higher shear causes higher proliferation rates [63]. Additionally, higher passages had a higher apoptotic rate than their lower passage counterparts. The proliferation in higher passages decreased in comparison to the lower passages ***(Figure 11)***, ***(Table 7)***. The potential cause for a low proliferation rate and higher apoptotic rates in higher passages could be senescence. Senescence is the life of the cell, and eventually how it stops proliferating and is programmed for cell death. Wagner et al., suggests the cellular pathways are disrupted by senescence, leading to an increase in apoptosis supporting the idea that cellular ageing plays a role in arteriosclerosis. Arteriosclerosis is the hardening of the arteries which is characterized by abnormal thickening. As previously stated, one of the comorbidities of Fontan failure is arterial remodeling [72]. Arteriosclerosis was found to have excessive cellular apoptosis in a study by Bennet et al. [73]. Although not completely understood, a connection between levels of VEGF and arteriosclerosis has also be investigated [26]. There was a statistical difference between the passages and their cell count. Passage 6 had

Table 7: Experiment 1- Final Cell Counts; Raw Data

		Passage		
		4	**6**	**12**
RPM	**0**	523000	471000	31400
		262000	126000	52300
		194000	110000	62800
	50	131000	246000	298000
		209000	262000	330000
		25000	377000	303000
	100	162000	94200	73200
		178000	173000	52300
		126000	575000	41900
	200	146000	215000	15700
		146000	204000	20900
		120000	251000	26200

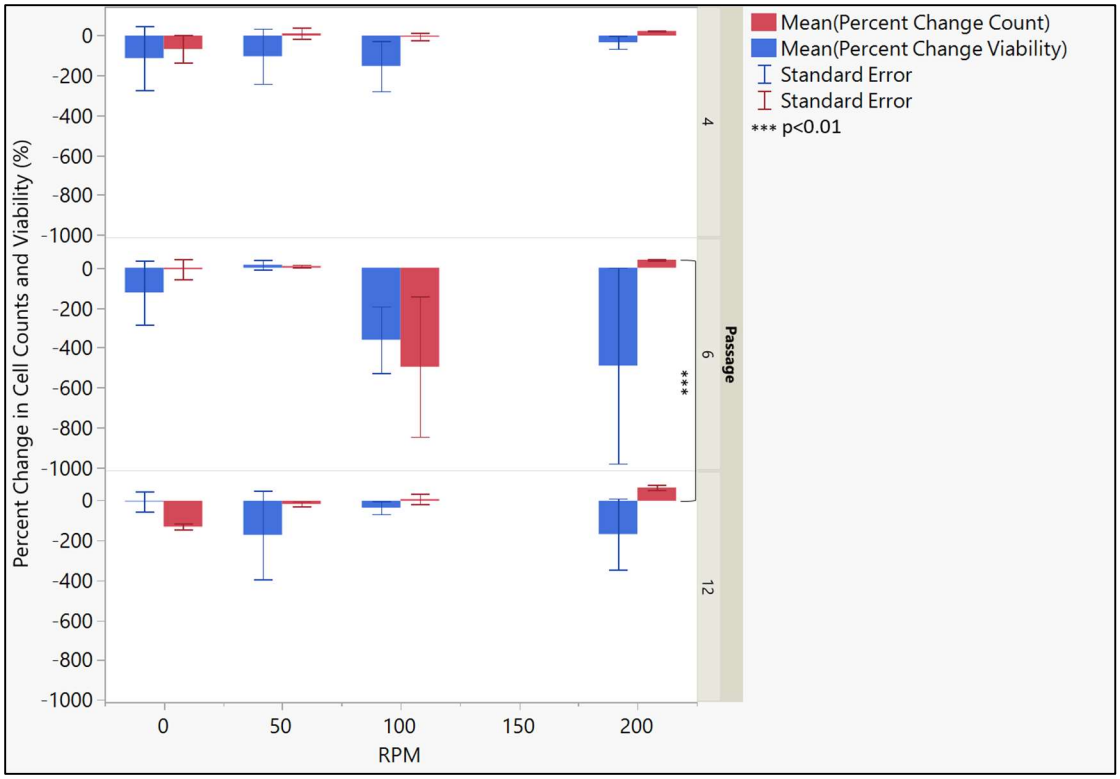

Figure 11: Experiment 1-Percent Change Cell Counts and Viability; There was a statistical significance between the cell counts for passages 6 and 12, with a p value of 0.0056.

the highest counts in comparison to passages 4 and 12. The statistical significance is specifically between passages 6 and 12. There is a potential connection to the doubling of age, in which senescence may be more noticeable. There is also a chance this is due to lack of experience with cell culture techniques, as there was no literature supporting this data. There was no statistical difference with viability.

Morphology

Cells were expected to lengthen and align in the direction of the shear stresses [48], [74]. The data collected aligned with this hypothesis, as the cells lengthened by approximately 58% and thinned by approximately -16% between 0 and 100 RPM. The morphology was significant between the dimensions of length and width. In addition, there was significance between passages 4 and 6 with a p value of 0.0043 between passages 6 and 12 with a p value of 0.0026, and between passages 4 and 12 with a p

value of 0.0001. ***Figure 12 B*)** represents the 200 RPM trial- the cells are seen aligning in the direction of the stresses and are generally more uniform in arrangement than the 0 RPM trial. This alignment occurs in healthy human hearts because the vasculature is maintaining homeostasis in favor of proper vasodilation and vasoconstriction. Particularly in Fontan patients, vasodilation is of more interest. Vasodilation widens blood vessels, increases blood flow, and decreases blood pressure. This helps with preventing hypoxia and pulmonary hypertension, which are some of the well-known comorbidities of Fontan Failure [75],[10]. Because the morphology of the lower RPMs does not match the morphology of healthy cells in the body, it may suggest that cell signaling is disrupted and cells are not producing the necessary markers to survive. When cells adopt this morphology, the cells develop stress fibers, serving as important cellular components for adhesion, migration, and contractility [76]. HPAECs in a healthy human body are typically exposed to steady unidirectional shear stress, so although the morphology aligned with literature, the orbital nature of the applied shear stresses is not an accurate representation of shear stress in the body [75].

Transcriptomics: Vascular Endothelial Growth Factor

There was no statistical difference RPM or passage regarding VEGF concentrations, however there are trends to be discussed. The function of the cell is linked to its morphology; therefore, it was hypothesized function would be altered. Lower concentrations of VEGF were measured in the higher RPM, however, this contradicts previous studies where VEGF concentration was expected to increase with shear. The VEGF concentration was expected to rise as a response to high shear [26],[27] (***Figure 13), (Table 8)***. Despite the opposite results, a potential cause for the lower concentration is that KLF2 has been shown to suppress the induction of VEGF in higher shear. There was also a higher concentration of VEGF in lower passages, in which the cells have not been passaged as many times. This may be connected to the senescence of primary human cells and that the cells lose function in higher passages [22], [77].

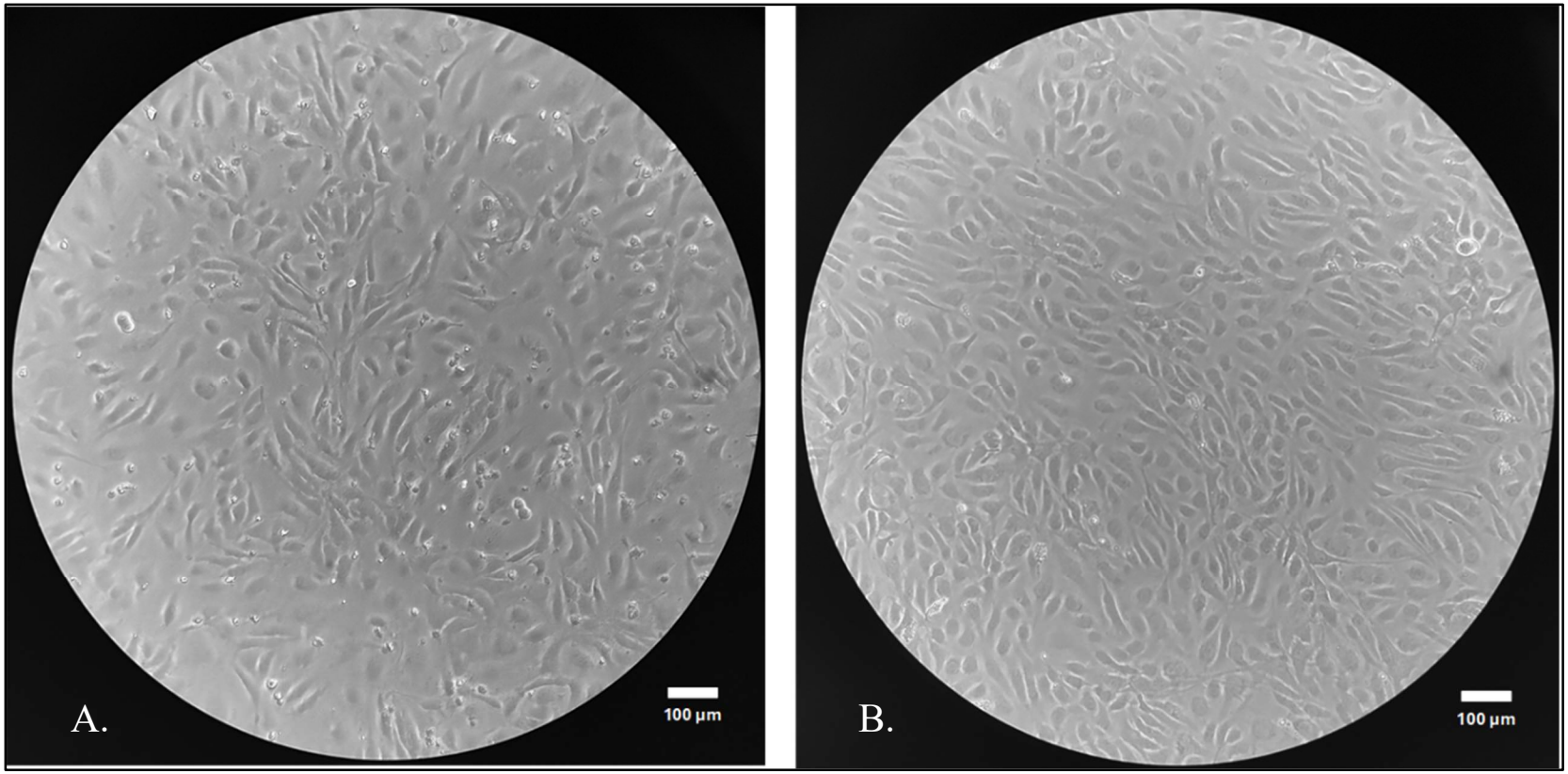

Figure 12: Experiment 1- Morphology Microscopy Images; A) 0 RPM, B) 200 RPM. Cell shape and pattern changes from A) to B)

*Table 8: Experiment 1- VEGF Concentration (*pg/mL*); Raw data for VEGF ELISA averaged between RPM and passage. Highest concentrations in passage 4 and 50 RPM.*

		RPM				AVERAGE
		0	**50**	**100**	**200**	
Passage	4	0.21	0.69	0.37	0.07	0.34
	6	0.18	0.42	0.08	0.31	0.25
	12	0.37	0.09	0.08	0.07	0.15
AVERAGE		0.25	0.40	0.18	0.15	

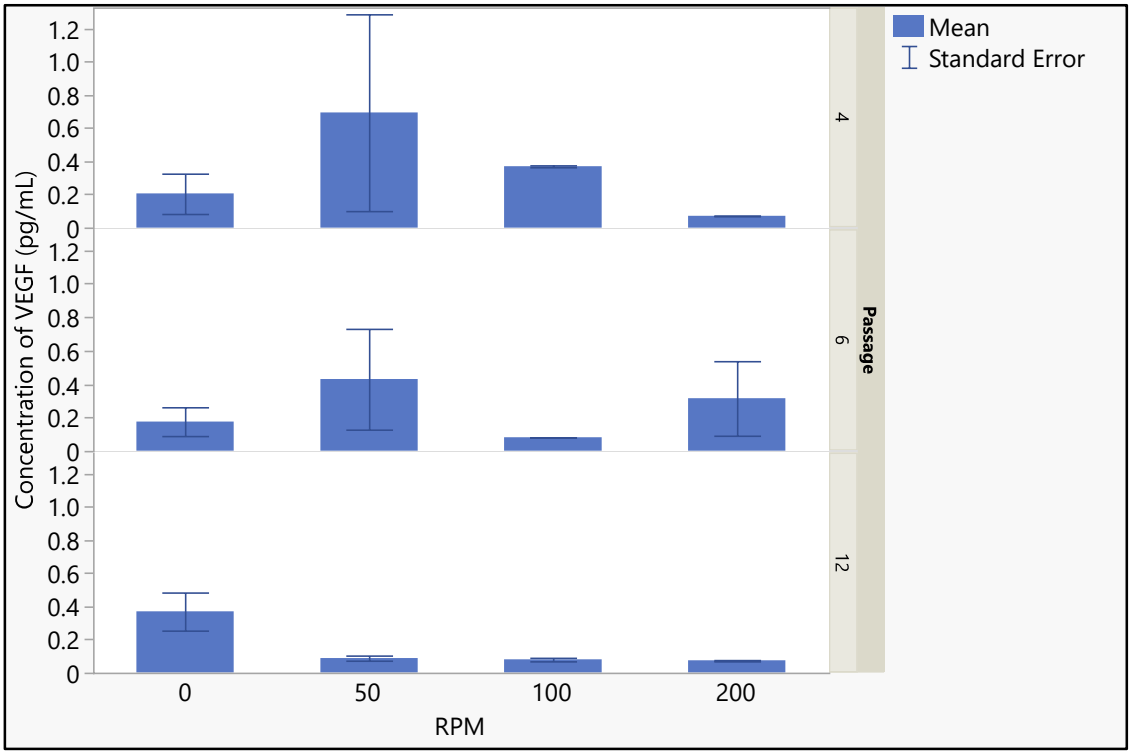

Figure 13: Experiment 1- VEGF Concentration (pg/mL); The highest concentration of VEGF was in passage 4 at 50 RPM. The lowest was in passage 12.

Final Experiment

For the final experiment in this thesis, the 6-well plates were swapped for 12-well plates for optimization of time and materials. Various passages were not tested, because there was no statistical significance between the collected data, and the scope of the project does not involve determining differences between the "age" of the cells. The maximum RPM was decreased from 200 to 100 in hope of replicating the Fontan shears more accurately. This led to the development of the experimental groups mentioned in the methodology section seen in ***Table 2***.

Computational Fluid Dynamics

Because the first experiment simulations were not as refined, the results showed that 200 RPM was representative of healthy human WSS. After completing the final CFD simulations it was found that the designated shear groups are significantly lower than expected. 100 RPM is most representative of average Fontan WSS although it is significantly lower. There is a correlation between decreases in RPM and decreases in WSS. Also, the oscillatory shear index (OSI) demonstrated values similar to the Fontan physiology, in which are averaging about 0.4-0.5 [78], [79] (***Table 9***) ***(Figure 14***). A value of OSI this high suggests that the flow over time drastically changes from unidirectional to oscillatory flow patterns. The surprising results of the final CFD simulations ***(Figure 15)*** would lead to revisiting the higher RPM cases. As noted, the first experiment CFD results showed that at 200 RPM, there was a fluid motion that exposed the cells to air potentially resulting in the corresponding cell counts and viability. It is now known that the magnitude of shear was not likely the issue, instead the volume of media. A rerun of the experiment at higher RPMs may be valuable to have a control group more similar to that of healthy human physiology. Nevertheless, molecular marker expression has shown changes in trend from low to high RPM, demonstrating that there may be a connection between WSS and molecular marker induction.

Cell Counts and Viability

The cell counts collected in the final round of experimentation were similar to past trials with a few key differences. The 75 RPM group produced the highest cell count

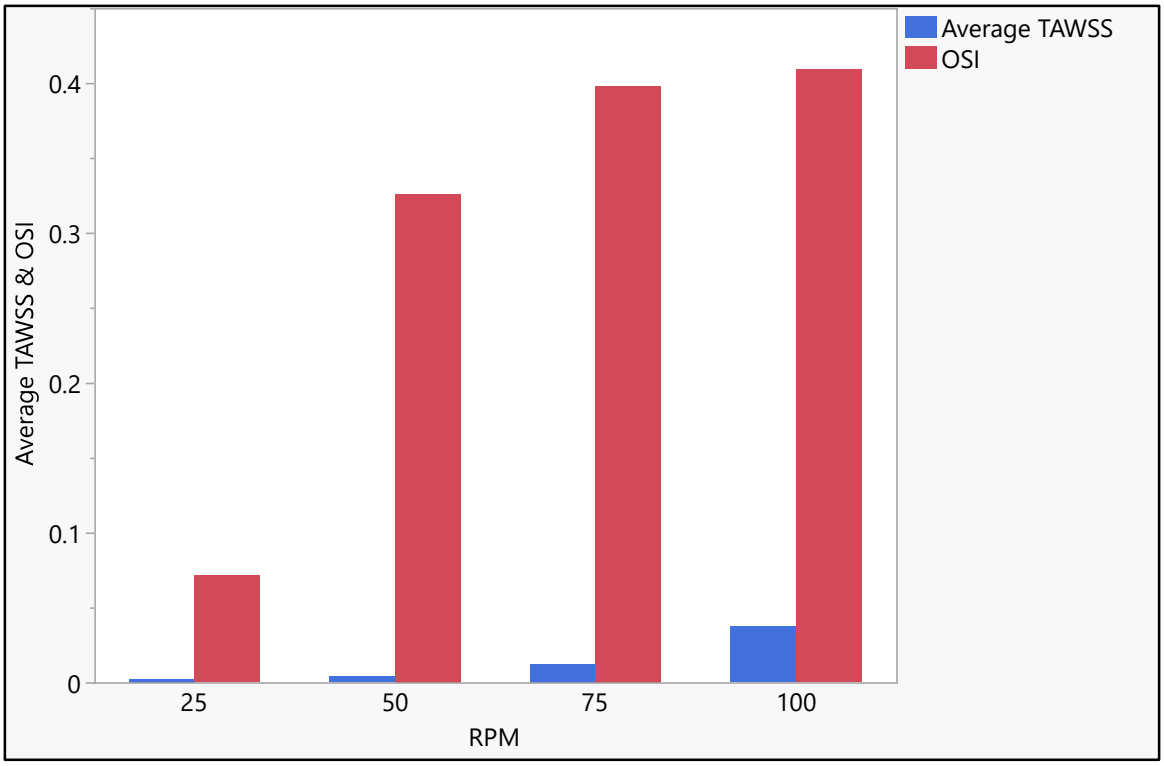

Figure 14: Final Experiment- TAWSS and OSI

Table 9: Final Experiment- Average Values from CFD Simulations; Values in the table are averaged over time and then averaged over the entire well plate.

RPM	Average TAWSS	Average Min TAWSS	Average Max TAWSS	Average TAWSS Std Dev	OSI
25	0.0021	0.0008	0.0042	0.0008	0.0713
50	0.0039	0.0007	0.0077	0.0016	0.3261
75	0.0124	0.0062	0.0182	0.0028	0.3979
100	0.0373	0.0231	0.0562	0.008	0.4088

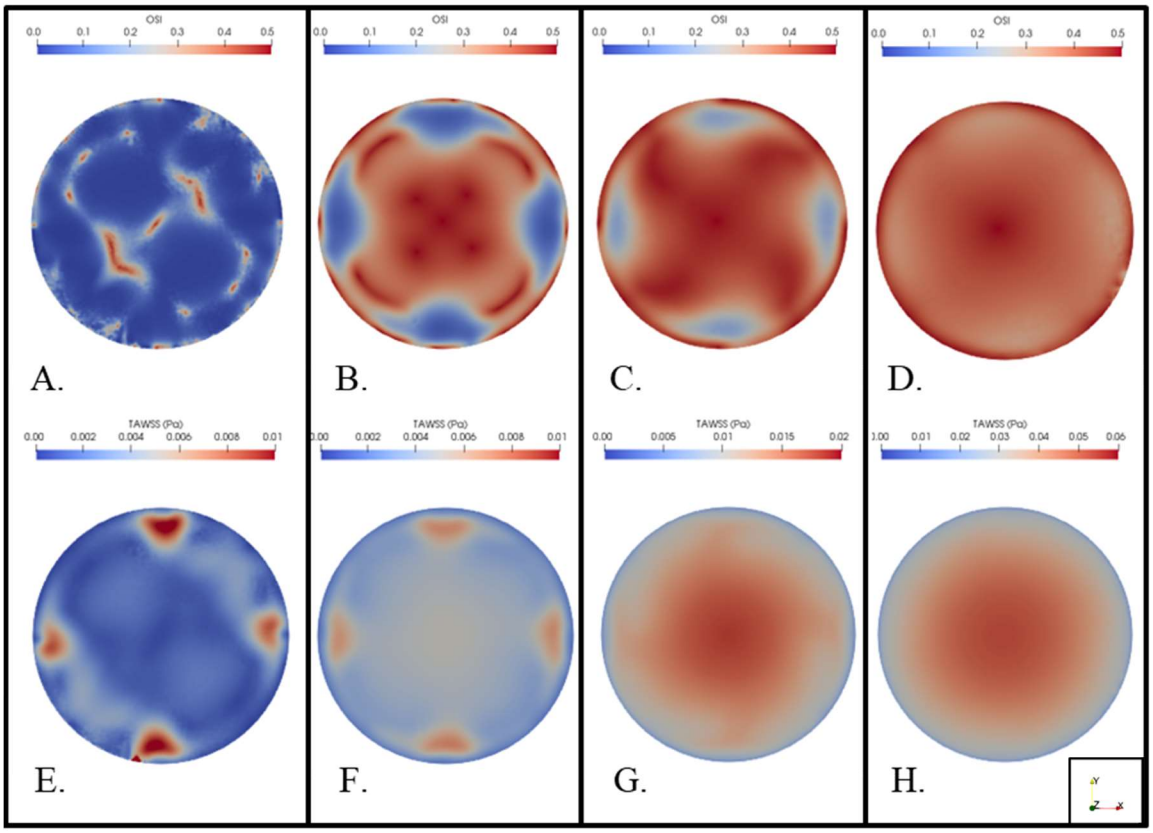

Figure 15: Final Experiment- Computational Fluid Dynamics; A) OSI 25 RPM, B) OSI 50 RPM, C) OSI 75 RPM, D) OSI 100 RPM, E) TAWSS 25 RPM, F) TAWSS 50 RPM, G) TAWSS 75 RPM, H) TAWSS 100 RPM

after applying the shear stresses. There is also a varied increase from 0 RPM to 100 RPM, which was expected to occur. However, what caused the peak at 75 RPM is not completely understood. The percent change in viability remains somewhat constant, except for the drop at 75 RPM ***(Table 10)***, ***(Figure 16)***. The drop may potentially be connected to the spike of cell counts. In a study by Fisher et al. it was determined that endothelial cell turnover is elevated in areas with complex flow, potentially explaining the low cell counts in 100 RPM, and low viability in each group, especially the 75 RPM. The increase in apoptosis causes varying responses in gene expression resulting in complex signaling cascades [80].

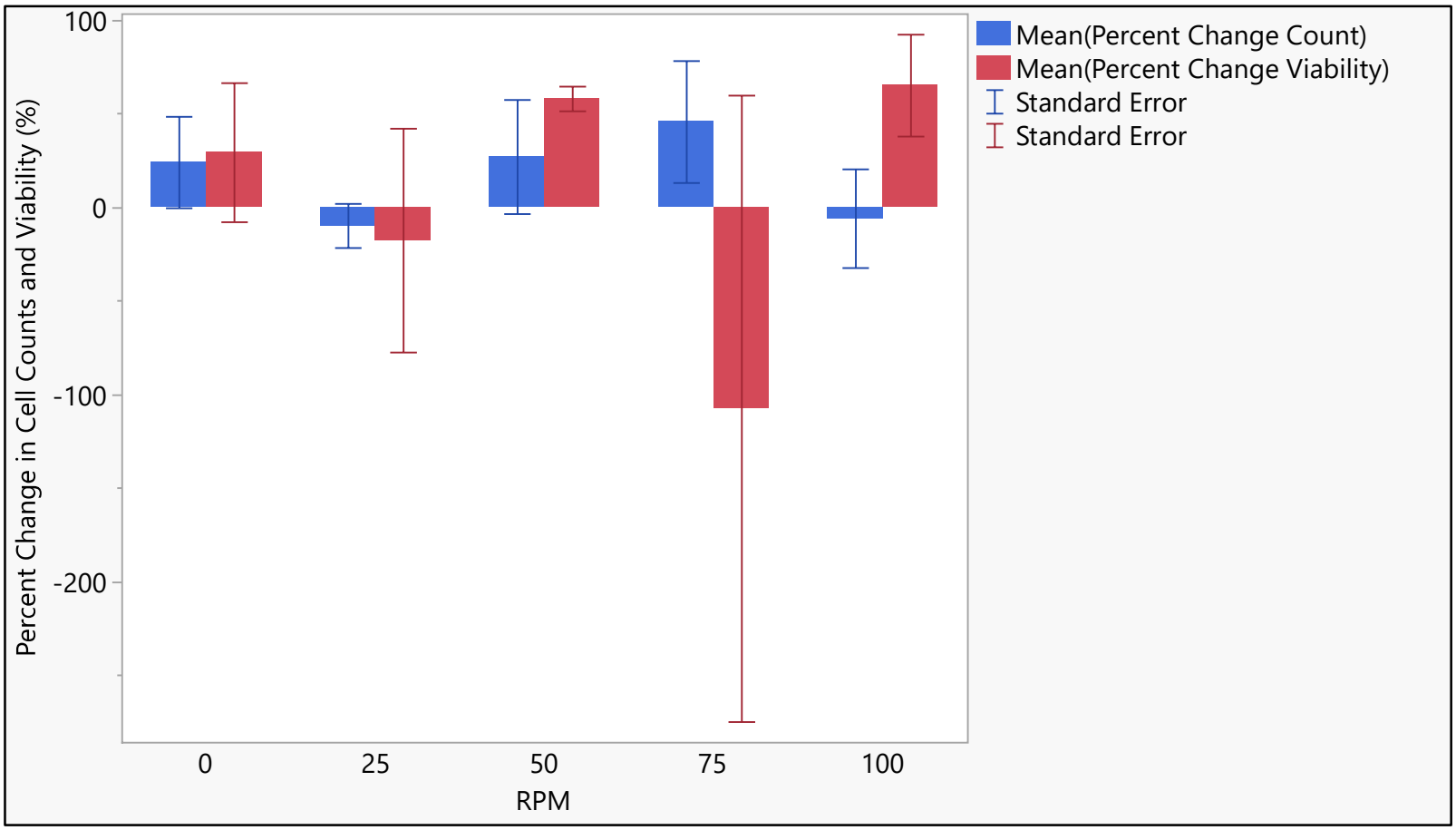

Figure 16: Final Experiment- Cell Count and Viability Percent Change; Largest percent change for both count and viability in 75 RPM

Table 10: Final Experiment- Counts and Viability; Raw Data

RPM	Count	Viability
0	106379	21.67
	153465	34.33
	116843	27
	200551	29.33
	111611	21.33
25	179624	38
	127307	25.67
	83708.4	21
	108123	25
	136026	28
50	111611	22
	235430	36.67
	294723	34
	247637	30.67
	206655	12.67
75	184856	12.67
	284260	12.67
	340065	23
	469116	33.67
	156953	34
100	97659.8	19.33
	99403.7	46
	184856	9.333
	151721	53.33
	127307	13.67

Morphology

Consistent with results from the preliminary study and experiment 1, the cells lengthened and aligned in the direction of the shear stresses. Cells lengthened by approximately 43.35% and thinned by approximately -25.78% between 0 and 100 RPM ***(Figure 18***). Microscopy images reveal the morphology of the cells to the human eye. At 0 RPM, the cells are more confluent, randomly arranged, and are normal in shape. When increasing RPM, the cells are more sparse, their morphology changes, and cells slightly arrange in a pattern (***Figure 17*** **A)** represents the stationary group, ***Figure 18*** **E**) represents the 100 RPM group). This pattern cannot be seen as clearly as in ***Figure 12*** with 200 RPM. From the results in the Final Experiment Cell Count and Viability section, it can be suggested this less confluent pattern of the cells in the higher RPM can be related to the higher apoptosis rates induced by the complex flow patterns, resulting in less viability.

Transcriptomics: Bulk RNA

The bulk RNA library formation was difficult to begin because the preliminary gel electrophoresis revealed that the RNA was degraded. The RNA integrity numbers (RIN) for the samples were below 5, which is not optimal. A proper RIN would be above 7. Possible sources for the degradation include the expiration date of the RNA kit, the freezing media of the cell samples, the cell counts, or the amount of time that the cells were frozen. After the process of elimination, the probable source of error is the freezing medium of the cells- the media was altered in order to prevent incorrect assay signaling. The lack of proper cryoprotectant likely resulted in the cells lysing prematurely and degrading the RNA.

Transcriptomics: Vascular Endothelial Growth Factor

Consistent with literature review and opposite to the unexpected results in experiment 1, VEGF concentration increased from low to high RPM (***Figure 19) (Table 11***). There is also a slight peak in concentration at 50 RPM, which suggests that this may be similar to Fontan stresses in the body. As previously stated, VEGF concentration increases with high laminar shear, which is healthy, and increases at low complex shear,

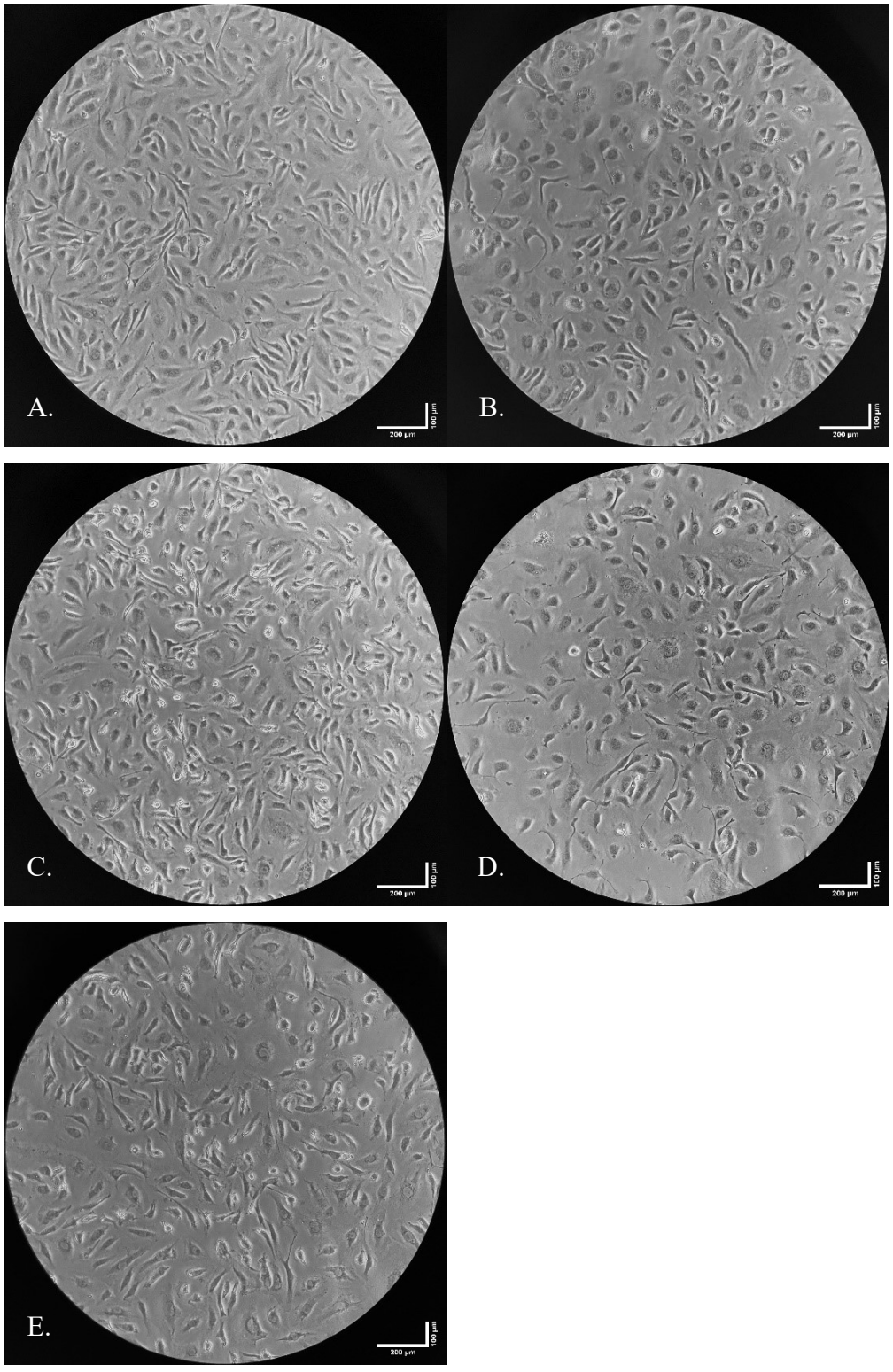

Figure 17: Final Experiment- Morphology Microscopy Images; A) 0 RPM, B) 25 RPM, C) 50 RPM, D) 75 RPM, E) 100 RPM.

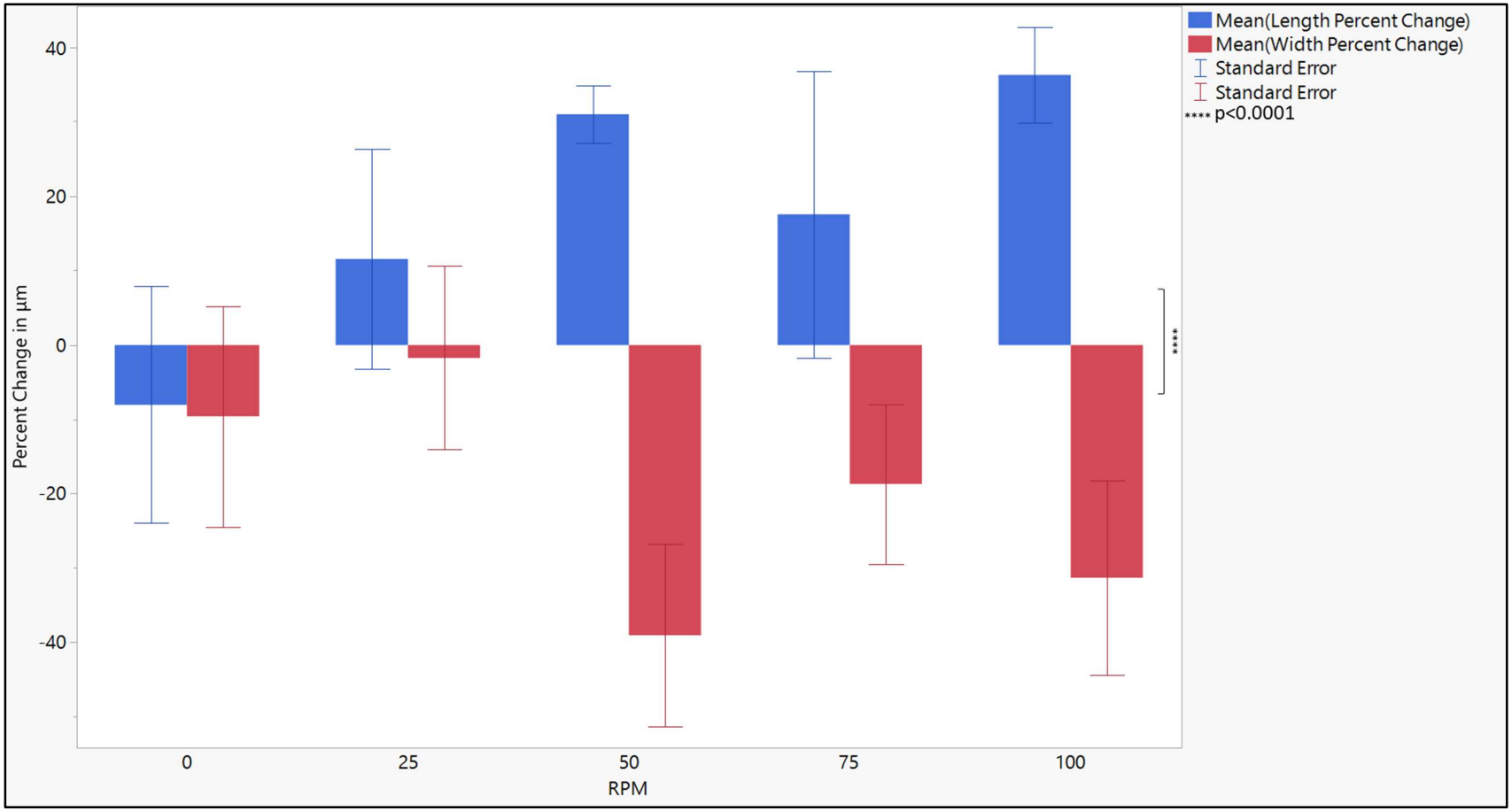

Figure 18: Final Experiment Morphology- percent change of length increased and width decreased toward 100 RPM. There was a statistical significance between length and width percent change with a p value of 0.0001.

.

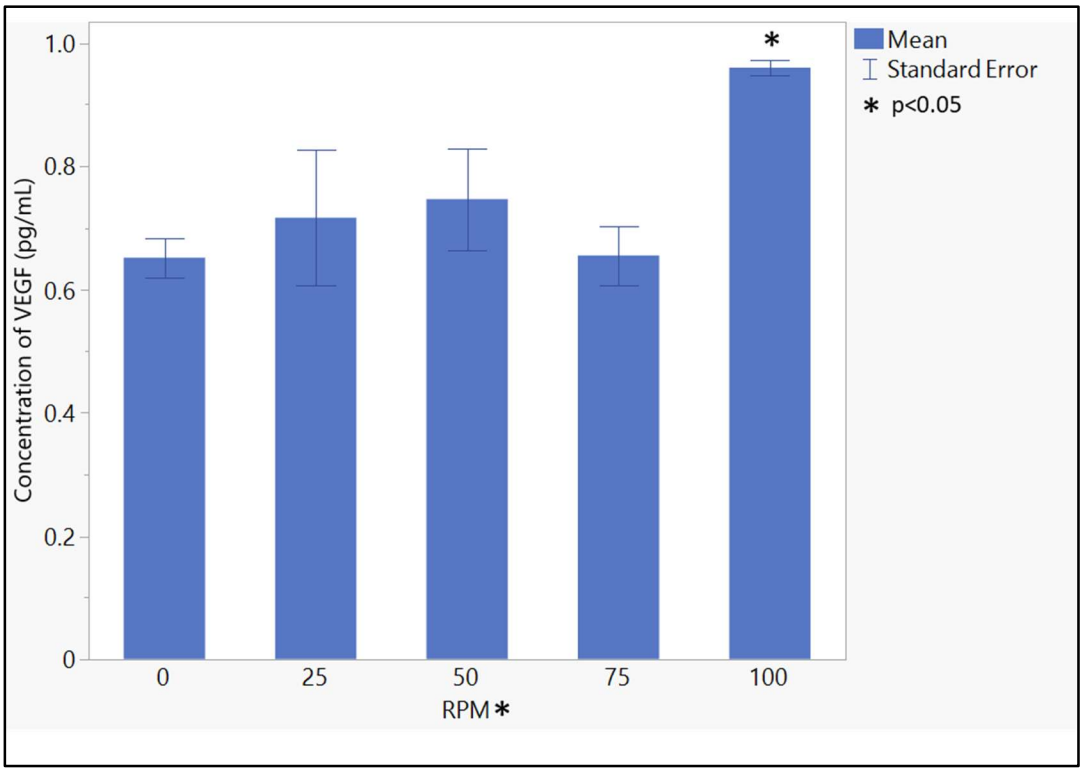

Figure 19: Final Experiment- VEGF Concentration (pg/mL); 100 RPM with a p value of 0.0270, and difference in RPM with a p value of 0.0463.

Table 11: Final Experiment- VEGF Concentration (pg/mL);

RPM	Concentration
0	0.7087
0	0.5999
0	0.6449
25	0.7799
25	0.8661
25	0.5024
50	0.8736
50	0.7724
50	0.5924
75	0.7124
75	0.6936
75	0.5587
100	0.9599
100	0.9823
100	0.9374

which is representative of the Fontan physiology [38], [39]. While it is contradictory that there are higher levels in healthy hearts, and abnormal hearts, there is a potential connection between the Fontan physiology and elevated levels of VEGF. Both of these correlations may be markers of angiogenesis, as this process occurs in an attempt to provide more oxygen to the body as a result of hypoxia [39]. This increase may also be cause by injury, in which the endothelial cells release VEGF, leading to pulmonary vascular remodeling in Fontan patients [38]. The remodeling occurs because of the signaling cascade that takes place between the HPAECs and smooth muscle cells- increasing the proliferation of the smooth muscle cells [38]. The remodeling as a result, is disordered [40].

Metabolomics: Nitric Oxide

The NO assay revealed results that also aligned with literature review. It was found that the concentration of NO increased with an increase in RPM (***Figure 20)*** ***(Table 12)***. NO is known to down regulate gene expression of adhesive proteins, to inhibit platelet adhesion and induce VEGF expression. The inhibition of platelet adhesion prevents aggregation and clotting of blood. This is healthy for the body, as it prevents plaque buildup and blood clots from forming. Therefore, it is possible that the downregulation of NO may play a role in the higher viscosity of Fontan blood in addition to the shear thinning properties of blood. NO has also been found to prevent smooth muscle cell proliferation, therefore preventing remodeling [30]. In the case of the Fontan physiology, eNOS, the signaling pathway for NO, is reduced as a result of pulmonary hypertension, resulting in the previous effects to be the opposite [29].

Metabolomics: Lipids

In the final experiment, the samples were tested for specific lipid species and general metabolites. Within the lipids category, the most prominent species were Digalactosyldiacylglycerol (DGDG) and fatty acids (FA). The highest percent changes involved DGDG, which is a lipid species that is typically found in plant chloroplasts, which potentially suggests that there may have been cell contamination in the 75 RPM group. DGDG is found in various types of cell contamination such as yeast or mold. Although there was no visible contamination during microscopy analysis, this reveals

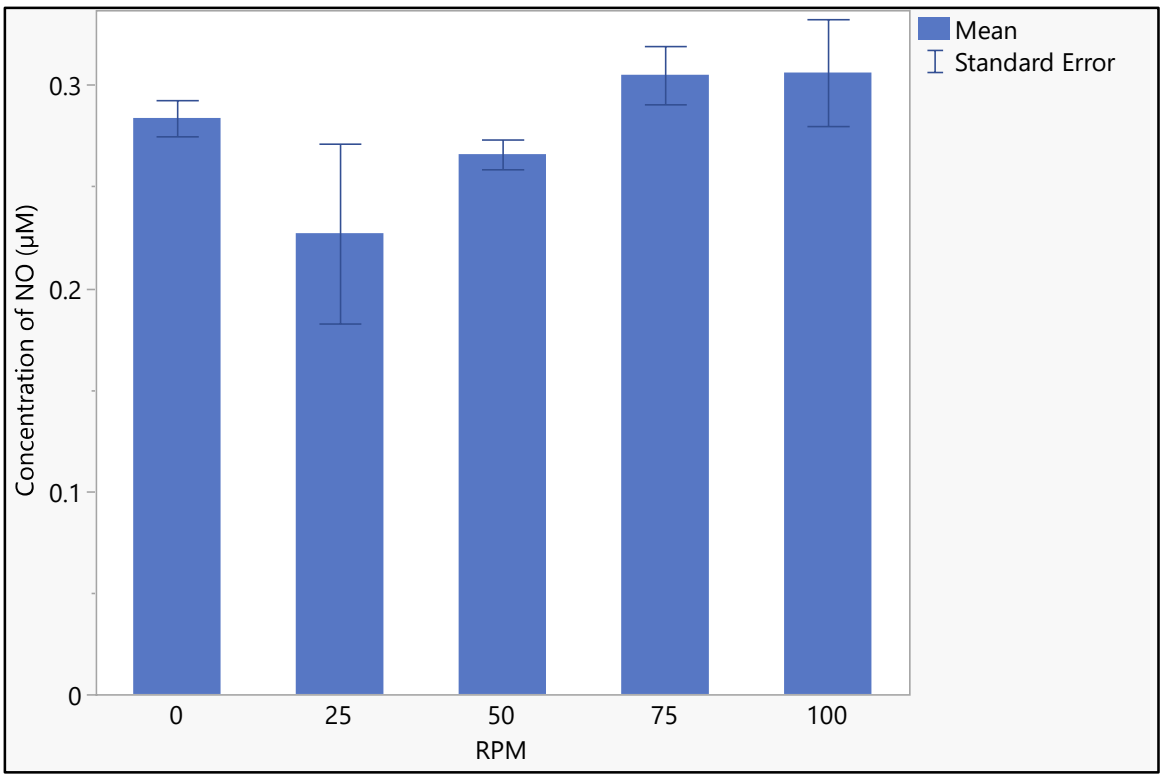

Figure 20: Final Experiment- NO Concentration (µM); Concentration increased from 25 to 100 RPM.

Table 12: Final Experiment- NO Concentration (µM); Raw data

RPM	Concentration
0	0.2942
0	0.2907
0	0.2659
25	0.2729
25	0.1382
25	0.2694
50	0.2800
50	0.2552
50	0.2623
75	0.2871
75	0.2942
75	0.3332
100	0.2729
100	0.2871
100	0.3580

why the previous results may have been altered, as contamination also results in cell dysfunction, and there may be signaling from these contaminants. Despite this potential discrepancy, DGDG lipids play a significant role in membrane morphology and NO regulation, as it acts like a bioregulator [81]. FA lipids can be converted by different pathways into various phospholipids such as the lipids found in the preliminary results. FA lipids are the building blocks to more specific lipid species, however FA lipids do play a critical role in the cardiovascular system (***Table 13***) [82]. The general trend was that lipids were downregulated at higher RPMs in contrast to the lower RPMs. For general metabolites, the largest percent changes were acetyl lysine and n-acetyl glutamine both of which have been linked to the implications of remodeling as well as CHD [83]. Additional metabolites along with their relationship to the cardiovascular system are found in ***Table 14****;* of interest, guanosine has been linked to NO regulation via the NO-cyclic guanosine monophosphate pathway (NO-cGMP). NO-cGMP plays a vital role in smooth muscle cells, platelet activity, cardiac contractility, and cell proliferation [84]. The metabolites were also downregulated at higher RPMs in comparison to lower RPMs. These lipids and metabolites were compared before and after application of the shear stresses *(****Figure 21***).

Developing a Collagen Co-Culture

The development of a collagen gel proved to be difficult, and this part of the study will be ongoing. There are multiple techniques for developing a collagen cell culture, as seen in the appendix. A collagen gel was the desired outcome for this study because of the goal to seed pulmonary artery smooth muscle cells into the gel, and then seed HPAECs on the top of the gel. This study design was to simulate a vessel wall more accurately. However, there were several failed attempts prior to obtaining just a collagen gel with no cells. The protocol as listed in the appendix was used, but adjustments to the measurements had to be made. These changes were made because the pH of the resulting collagen gels was either too acidic or basic. Proper gelling of the collagen relies on the pH to be between 7-8, and this is also necessary for the survival of the HPAECs and future smooth muscle cells. The pH must be similar to that of blood, which is 7.4. With the improper pH, the collagen gels were not solidifying and resulted in a broken layer

Table 13: Final Experiment- Significant Lipids and the Relationship to the Cardiovascular System

Lipid	p Value	Relation
FA 20:3	0.0003	Cardiovascular mortality [85]
FA 22:6	0.0033	Cardiomyopathy, remodeling, heart failure [70], [86]
FA 22:5	0.0108	Cardiomyopathy, remodeling [86]
FA 22:4	0.0164	Cardiomyopathy, remodeling [86]
PC 32:1	0.0441	Hypertension [69]

Table 14: Final Experiment- Significant Metabolites and the Relationship to the Cardiovascular System

Metabolite	p Value	Relation
Guanosine	0.0026	Hypertension, congenital heart disease, Fontan treatment [84], [87]
Deoxyuridine	0.0111	Proliferation changes, congenital heart disease [88]
2-hydroxyglutaric acid	0.0478	Decreased cardiac output, decline in contractile function, cardiomyopathy [89], [90]

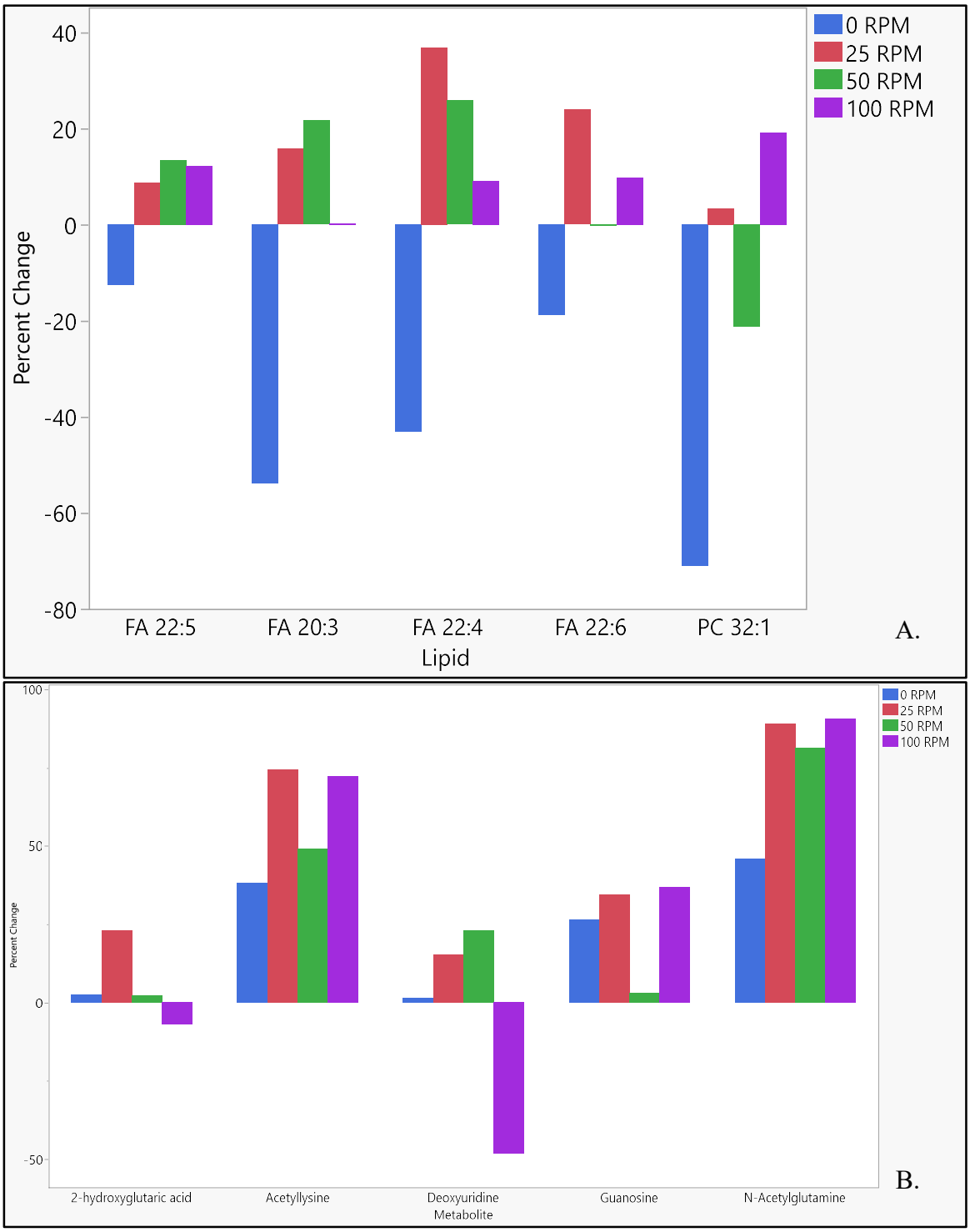

Figure 21: Final Experiment- LCMS Results Percent Change; A) Lipids B) Metabolites

floating in cell media. To adjust the pH, different volumes of media, PBS, and chemicals were used to determine the proper ratio. Without any success, a series of literature had to be reviewed for guidance on how to create a collagen gel. Despite this setback, steps were created on what not to do (***Figure 22)***.

Limitations

In this work, there are limitations. For example, cell culture was a new technique in the Crouch Imaging Lab. Another limitation is the environment in which the experiment took place. Although set up for cell culture, the lab is suboptimal due to the location, which is the interior of a public workspace without locks, and the walls do not go to the ceiling. This proves difficult to maintain sterility and may be a potential cause for the discovered contamination. Additionally, the orbital shaker has limitations in methodology because it does not provide consistent stresses throughout the sample. The center and exterior wall cells experience different magnitudes of stress, potentially altering results. There is also the aspect that Fontan physiology varies widely amongst patients- no two patients will have the same results from their surgery. Because there are so many physiologies, there would be several different molecular markers induced for each patient, and similarities would need to be noted for multiple patients to create a conclusion regarding the Fontan markers. Also, standard errors may be large for some results because of limitations from primary human cell culture. For example, the cells used in this thesis, although from the same lot and source, come from two separate stock orders. This may have resulted in variability causing inconsistency with contamination.

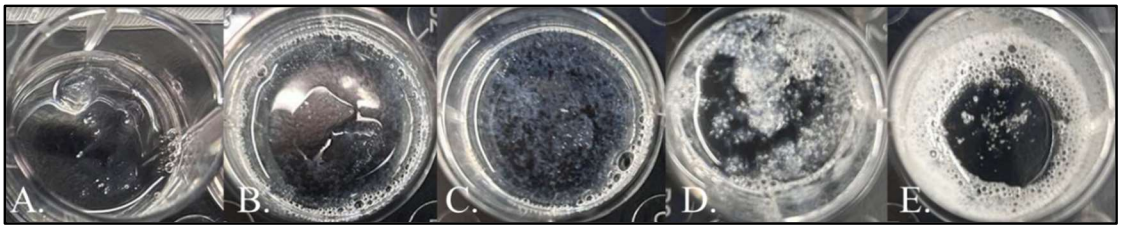

Figure 22: Final Experiment- Collagen gel attempts; A) Clump of collagen, B) Broken collagen gel, C) Denaturized collagen, D) Bubbling and broken collagen gel, E) Bubbling collagen solution

CHAPTER FIVE: Conclusions and Recommendations for Future Work

Conclusions

The data collected over the course of this thesis indicates the potential connection between varying shear stresses and molecular markers. There is evidence that the collected data has relevance to pulmonary hypertension, pulmonary vascular resistance, and pulmonary vascular remodeling caused by shear stresses. With further development, this study has the potential to connect the molecular markers to Fontan Failure. The concentrations of VEGF and NO align with trends found in people with CHD and the Fontan procedure, in which they increase and decrease at lower levels of shear stresses respectively. Metabolites and specific lipids discovered also have relation to congenital heart disease, pulmonary hypertension, and contractile dysfunction. Regarding the bulk RNA attempt, it was concluded that the storage media likely lysed the cells, degrading the RNA- therefore, the trials will be repeated to correct this. The repetition of the trials will also allow for potential correction of the 75 RPM group, as the results for this group were abnormal in each test. However, there is evidence that the tested molecular markers do change with a change in WSS, ultimately demonstrating the need for further refining of this project.

Future Work

Collagen Co-Culture

This project is expected to be ongoing to potentially lead to better diagnostics and therapeutics for Fontan failure. To do this, further development of collagen co-culture will be required. In a study by Ziegler et. Al, the authors utilize a method of seeding smooth muscle cells into the collagen gel and then seeded the HPAECs on the gel (***Figure 23***) [60]. This would simulate anatomy closer to that of the arteries because of the cellular layers that make up the vessel wall and reveal information about cellular signaling between cell types. Also, at low flow rates in the body, it is the collagen that determines organization of the endothelial cells. Fisher et. al demonstrated the importance of collagen regarding alignment and morphology. [80]. This is of interest because mass spectrometry imaging (MSI) analysis could be completed on the collected samples to reveal spatial lipidomic data.

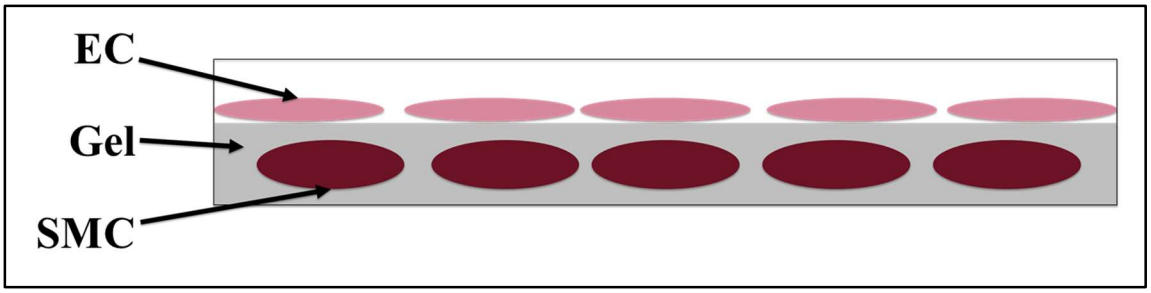

Figure 23: Collagen Co-Culture Schematic- Endothelial cells seeded on top of collagen gel containing embedded smooth muscle cells.

MSI and Preparation

Mass spectrometry imaging (MSI) gives insight into spatial distribution of biological samples. MSI can detect hundreds of molecules with no prior knowledge of the molecules present [17]. With the collagen co-culture, the MSI would provide insight into cellular signaling between cell types by showing the distribution of lipids in a cross section of the collagen. Prior to the completion of the MSI, the development of a collection and fixation preparation protocol would need to be determined. The collagen samples could be removed via razor blade and then sectioned in quarters for a more manageable size. Fixation and preparation would entail the comparison of formalin fixed paraffin embedding, flash freezing, or gelatin embedding samples to discover the best methodology of cell culture prep for MSI. The "golden standard" is fixed paraffin embedding. This is because of its properties to preserve features and results in minimum decay of the cells during long term storage [17]. Flash freezing is where samples are frozen immediately by liquid nitrogen. This method limits degradation of biomolecules, which is best for MSI [17]. Gelatin embedding involves placing samples in liquid gelatin solution and allowing it to solidify for sectioning. Gelatin embedding is a good alternative because it minimizes matric crystal formation and background signal [91]. The varying preparation methods need to be compared to determine the best option for MSI.

3D Culture

A step will also need to be taken to more accurately represent the shape of the pulmonary artery and Fontan physiology in the culture vessel. The anatomy and stresses

could be accomplished by utilizing a tube and pump system to represent the artery and blood flow, which could eventually be developed into a full heart system. HPAECs could be cultured on the interior of the tube, and media ran through the tube with a pump similar to that of Sato et al. [92]. A three-dimensional culture would be beneficial as well- utilizing a Fontan physiology mold to simulate the shear stresses. As per work done by Dr. Bryan Good, a silicone model of Fontan anatomy could be 3D printed and placed in a circulatory flow loop (***Figure 24***). These methodologies would overcome previous limitations of Fontan research by studying patient specific anatomy and the effect on endothelial dysfunction.

Viscosity

The media used in this thesis is less viscous than blood. Precisely, the viscosity of the media is approximately 0.9 centipoise (cP) which is lower than blood at 3.5 cP. Viscosity refers to the fluid's resistance to flow, and in the Fontan system, blood is more viscous. Blood is more viscous in the Fontan anatomy because the shear stress is lower- this is due to blood being thinning. [20], [93]. Higher viscosity causes more pulmonary

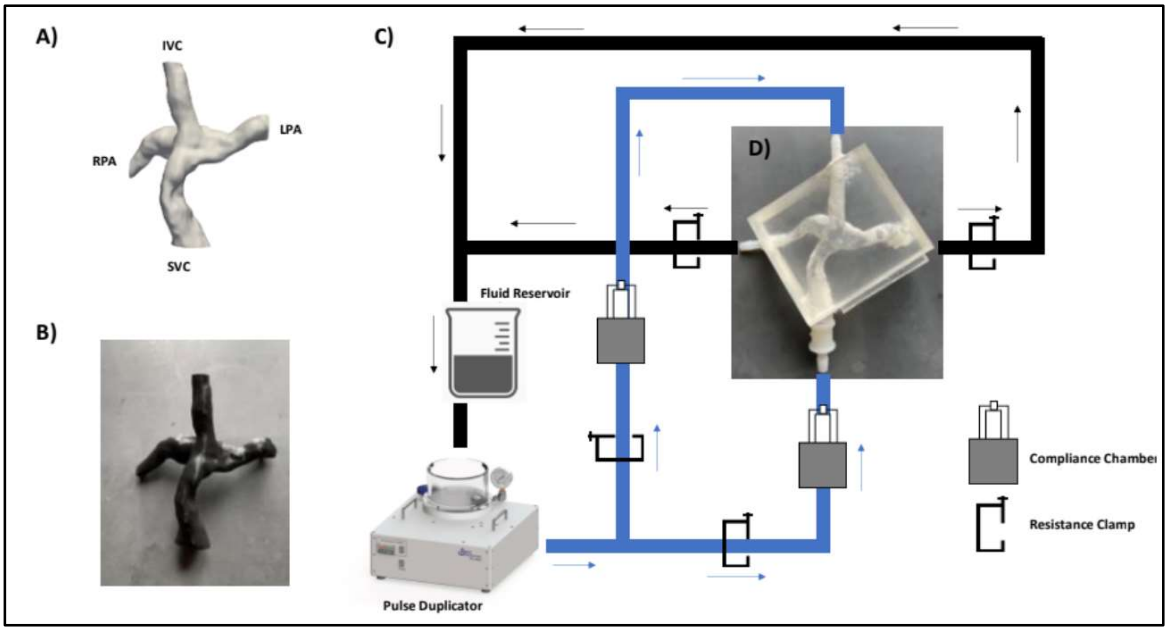

Figure 24: 3D Culture Model; A) Patient TCPC Cad Model, B) 3D Printed TCPC Model, C) MCFL with D) silicone TCP Model Incorporated

vascular resistance, potentially contributing to pulmonary hypertension in Fontan survivors. To accomplish the adjustment of viscosity, 4% high molecular dextran would be added to the media. The change of the media viscosity would enhance the applicability to Fontan physiology and its correlation to PVR.

Patient Specific Analysis

Currently, there is an ongoing collaboration with the University of Tennessee Health Sciences Center (UTHSC) in Memphis, Tennessee. The collaborators are willing to provide patient data such as catheterization labs, blood samples, and potentially hearts removed during transplant. Data as such would provide the opportunity to complete patient specific analysis. Magnetic resonance imaging (MRI) could be used to create shear stress simulations, which could eventually be translated into cell culture modeling. The blood samples will be analyzed with LCMS, ELISA, and Bulk RNA to compare to previously in vitro cell culture collected data. This could provide insight and comparison of potential biomarkers of Fontan Failure. The hearts would in an invaluable asset, as the hearts could be prepared for imaging, and primary cell collection for culture. Although difficult, primary cell culture from formalin fixed hearts utilizing the correct protocols. It is important to consider that the resulting Fontan physiology varies amongst patients, and obtaining real life samples would contribute greatly to the development of this project.

LIST OF REFERENCES

[1] S. Yagel *et al.*, "Congenital Heart Defects: Natural Course and In Utero Development," *Circulation*, vol. 96, no. 2, pp. 550–555, Jul. 1997, doi: 10.1161/01.CIR.96.2.550.

[2] L. E. Parker, L. M. Kurzlechner, and A. P. Landstrom, "Induced Pluripotent Stem Cell–Based Modeling of Single-Ventricle Congenital Heart Diseases," *Curr. Cardiol. Rep.*, vol. 25, no. 5, pp. 295–305, May 2023, doi: 10.1007/s11886-023-01852-3.

[3] P. S. Rao, "Single Ventricle—A Comprehensive Review," *Children*, vol. 8, no. 6, p. 441, May 2021, doi: 10.3390/children8060441.

[4] American Heart Association, "Single Ventricle Defects," Mar. 2022.

[5] J. Monaco, A. Khanna, and P. Khazanie, "Transplant and mechanical circulatory support in patients with adult congenital heart disease," *Heart Fail Rev*, vol. 25, pp. 671–683, 2020.

[6] M. Lee, *Fontan Completion*. StatPearls. [Online]. Available: https://www.ncbi.nlm.nih.gov/books/NBK558950/

[7] T. B. Fredenburg, T. R. Johnson, and M. D. Cohen, "The Fontan Procedure: Anatomy, Complications, and Manifestations of Failure," *RadioGraphics*, vol. 31, no. 2, pp. 453–463, Mar. 2011, doi: 10.1148/rg.312105027.

[8] W. M. Gersony, "Fontan Operation After 3 Decades: What We Have Learned," *Circulation*, vol. 117, no. 1, pp. 13–15, Jan. 2008, doi: 10.1161/CIRCULATIONAHA.107.748566.

[9] A. C. Egbe, "Predictors of procedural complications in adult Fontan patients undergoing non-cardiac procedures," *Heart*, vol. 103, pp. 1813–1820, 2017.

[10] A. C. Egbe, W. R. Miranda, A. E. Ali, J. A. Dearani, A. Hsu, and H. M. Connolly, "Clinical characteristics and outcomes in middle-aged Fontan patients," *Int. J. Cardiol.*, vol. 418, p. 132658, Jan. 2025, doi: 10.1016/j.ijcard.2024.132658.

[11] C. Schilling *et al.*, "The Fontan epidemic: Population projections from the Australia and New Zealand Fontan Registry," *Int. J. Cardiol.*, vol. 219, pp. 14–19, Sep. 2016, doi: 10.1016/j.ijcard.2016.05.035.

[12] S. S. M. Bossers, "Long-Term Serial Follow-Up of Pulmonary Artery Size and Wall Shear Stress in Fontan Patients," *Pediatr Cardiol*, vol. 37, pp. 637–645, 2016.

[13] A. Enabnit and A. Warren, "Pulmonary Vascular Resistance: Understanding the Physiology of Pulmonary Blood Flow Regulation," *Dove Med*, Jul. 2023.

[14] R. M. Tuder, “Pulmonary vascular remodeling in pulmonary hypertension,” *Cell Tissue Res.*, vol. 367, no. 3, pp. 643–649, Mar. 2017, doi: 10.1007/s00441-016-2539-y.

[15] A. Postles, A. R. Clark, and M. H. Tawhai, “Dynamic blood flow and wall shear stress in pulmonary hypertensive disease,” in *2014 36th Annual International Conference of the IEEE Engineering in Medicine and Biology Society*, Chicago, IL: IEEE, Aug. 2014, pp. 5671–5674. doi: 10.1109/EMBC.2014.6944914.

[16] J. Totoń-Żurańska, T. P. Mikolajczyk, B. Saju, and T. J. Guzik, “Vascular remodelling in cardiovascular diseases: hypertension, oxidation, and inflammation,” *Clin. Sci.*, vol. 138, no. 13, pp. 817–850, Jul. 2024, doi: 10.1042/CS20220797.

[17] K. Ščupáková *et al.*, “Cellular resolution in clinical MALDI mass spectrometry imaging: the latest advancements and current challenges,” *Clin. Chem. Lab. Med. CCLM*, vol. 58, no. 6, pp. 914–929, Jun. 2020, doi: 10.1515/cclm-2019-0858.

[18] R. Klabunde, “Cardiovascular Physiology Concepts,” *CVPhysiology*, [Online]. Available: https://cvphysiology.com/hemodynamics/h003

[19] J. Widrich, “Physiology, Pulmonary Vascular Resistance,” *Natl. Cent. Biotechnol. Inf.*.

[20] Z. Wei *et al.*, “Non-Newtonian Effects on Patient-Specific Modeling of Fontan Hemodynamics,” *Ann. Biomed. Eng.*, vol. 48, no. 8, pp. 2204–2217, Aug. 2020, doi: 10.1007/s10439-020-02527-8.

[21] R. S. Seymour, Q. Hu, and E. P. Snelling, “Blood flow rate and wall shear stress in seven major cephalic arteries of humans,” *J. Anat.*, vol. 236, no. 3, pp. 522–530, Mar. 2020, doi: 10.1111/joa.13119.

[22] D. A. Chistiakov, A. N. Orekhov, and Y. V. Bobryshev, “Effects of shear stress on endothelial cells: go with the flow,” *Acta Physiol.*, vol. 219, no. 2, pp. 382–408, Feb. 2017, doi: 10.1111/apha.12725.

[23] A. A. Nava and V. A. Arboleda, “The omics era: a nexus of untapped potential for Mendelian chromatinopathies,” *Hum. Genet.*, vol. 143, no. 4, pp. 475–495, Apr. 2024, doi: 10.1007/s00439-023-02560-2.

[24] T. Haukaas, L. Euceda, G. Giskeødegård, and T. Bathen, “Metabolic Portraits of Breast Cancer by HR MAS MR Spectroscopy of Intact Tissue Samples,” *Metabolites*, vol. 7, no. 2, p. 18, May 2017, doi: 10.3390/metabo7020018.

[25] E. Van Den Bosch *et al.*, "Associations Between Blood Biomarkers, Cardiac Function, and Adverse Outcome in a Young Fontan Cohort," *J. Am. Heart Assoc.*, vol. 10, no. 5, p. e015022, Mar. 2021, doi: 10.1161/JAHA.119.015022.

[26] K. Florek, D. Mendyka, and K. Gomułka, "Vascular Endothelial Growth Factor (VEGF) and Its Role in the Cardiovascular System," *Biomedicines*, vol. 12, no. 5, p. 1055, May 2024, doi: 10.3390/biomedicines12051055.

[27] Y. Ootaki, M. Yamaguchi, N. Yoshimura, S. Oka, M. Yoshida, and T. Hasegawa, "Vascular endothelial growth factor in children with congenital heart disease," *Ann. Thorac. Surg.*, vol. 75, no. 5, pp. 1523–1526, May 2003, doi: 10.1016/S0003-4975(02)04814-2.

[28] M. Feucht, B. Christ, and J. Wilting, "VEGF induces cardiovascular malformation and embryonic lethality," *Am. J. Pathol.*, vol. 151, no. 5, pp. 1407–1416, Nov. 1997.

[29] M. Lévy, C. Danel, A.-M. Laval, F. Leca, P. R. Vouhé, and D. Israël-Biet, "Nitric oxide synthase expression by pulmonary arteries: A predictive marker of Fontan procedure outcome?," *J. Thorac. Cardiovasc. Surg.*, vol. 125, no. 5, pp. 1083–1090, May 2003, doi: 10.1067/mtc.2003.193.

[30] K. Naseem, "The role of nitric oxide in cardiovascular diseases," *Mol. Aspects Med.*, vol. 26, no. 1–2, pp. 33–65, Apr. 2005, doi: 10.1016/j.mam.2004.09.003.

[31] C. R. Ferreiro *et al.*, "Influence of Hypoxia on Nitric Oxide Synthase Activity and Gene Expression in Children With Congenital Heart Disease: A Novel Pathophysiological Adaptive Mechanism," *Circulation*, vol. 103, no. 18, pp. 2272–2276, May 2001, doi: 10.1161/01.CIR.103.18.2272.

[32] D. Journois, P. Pouard, P. Mauriat, T. Malhere, P. Vouhe, and D. Safran, "Inhaled nitric oxide as a therapy for pulmonary hypertension after operations for congenital heart defects," *J. Thorac. Cardiovasc. Surg.*, vol. 107, no. 4, pp. 1129–1135, Apr. 1994, doi: 10.1016/S0022-5223(94)70390-6.

[33] G. Van Meer and A. I. P. M. De Kroon, "Lipid map of the mammalian cell," *J. Cell Sci.*, vol. 124, no. 1, pp. 5–8, Jan. 2011, doi: 10.1242/jcs.071233.

[34] E. Calzada, O. Onguka, and S. M. Claypool, "Phosphatidylethanolamine Metabolism in Health and Disease," in *International Review of Cell and Molecular Biology*, vol. 321, Elsevier, 2016, pp. 29–88. doi: 10.1016/bs.ircmb.2015.10.001.

[35] B. Nordestgaard, *Triglycerides and cardiovascular disease*, 9943rd ed., vol. 384. The Lancet.

[36] V. Pelouch, M. Milerová, B. Hučín, M. Adamcová, B. Panušková, and J. Škovránek, "Protein and Phospholipids Composition of Human Myocardium in Children with Congenital Heart Disease," in *Frontiers in Cardiovascular Health*, vol. 9, N. S. Dhalla, A. Chockalingam, H. I. Berkowitz, and P. K. Singal, Eds., in Progress in Experimental Cardiology, vol. 9. , Boston, MA: Springer US, 2003, pp. 37–53. doi: 10.1007/978-1-4615-0455-9_4.

[37] F. Takaesu *et al.*, "Transcriptomic analysis of circulating extracellular vesicles during the perioperative period of Fontan and Glenn surgery," *Npj Cardiovasc. Health*, vol. 1, no. 1, p. 36, Dec. 2024, doi: 10.1038/s44325-024-00039-1.

[38] C. Evans, "Endothelial cells in the pathogenesis of pulmonary arterial hypertension," *Eur. Respir. J.*.

[39] A. Saraf *et al.*, "Biomarker profile in stable Fontan patients," *Int. J. Cardiol.*, vol. 305, pp. 56–62, Apr. 2020, doi: 10.1016/j.ijcard.2020.01.012.

[40] R. Tobal *et al.*, "Vascular Remodeling in Pulmonary Arterial Hypertension: The Potential Involvement of Innate and Adaptive Immunity," *Front. Med.*, vol. 8, p. 806899, Dec. 2021, doi: 10.3389/fmed.2021.806899.

[41] U. Förstermann and T. Münzel, "Endothelial Nitric Oxide Synthase in Vascular Disease: From Marvel to Menace," *Circulation*, vol. 113, no. 13, pp. 1708–1714, Apr. 2006, doi: 10.1161/CIRCULATIONAHA.105.602532.

[42] M. Michel *et al.*, "Targeted metabolomic analysis of serum phospholipid and acylcarnitine in the adult Fontan patient with a dominant left ventricle," *Ther. Adv. Chronic Dis.*, vol. 11, p. 2040622320916031, Jan. 2020, doi: 10.1177/2040622320916031.

[43] S. Talwar, S. P. Marathe, S. K. Choudhary, and B. Airan, "Where are we after 50 years of the Fontan operation?," *Indian J. Thorac. Cardiovasc. Surg.*, vol. 37, no. S1, pp. 42–53, Jan. 2021, doi: 10.1007/s12055-019-00906-y.

[44] F. M. Booyse, B. J. Sedlak, and M. E. Rafelson, "Culture of Arterial Endothelial Cells: Characterization and Growth of Bovine Aortic Cells," *Thromb. Haemost.*, vol. 34, no. 03, pp. 825–839, 1975, doi: 10.1055/s-0038-1654001.

[45] S. Chatterjee, A.-B. Al-Mehdi, I. Levitan, T. Stevens, and A. B. Fisher, “Shear stress increases expression of a K_{ATP} channel in rat and bovine pulmonary vascular endothelial cells,” *Am. J. Physiol.-Cell Physiol.*, vol. 285, no. 4, pp. C959–C967, Oct. 2003, doi: 10.1152/ajpcell.00511.2002.

[46] R. J. Dekker *et al.*, “Prolonged fluid shear stress induces a distinct set of endothelial cell genes, most specifically lung Krüppel-like factor (KLF2),” *Blood*, vol. 100, no. 5, pp. 1689–1698, Sep. 2002, doi: 10.1182/blood-2002-01-0046.

[47] S. Hemming, D. Cakouros, and S. Gronthos, “Detachment of Mesenchymal Stem Cells with Trypsin/EDTA Has No Effect on Apoptosis Detection,” *Stem Cells*, vol. 32, no. 7, pp. 1991–1992, Jul. 2014, doi: 10.1002/stem.1710.

[48] K.-A. Norton and A. S. Popel, “Effects of endothelial cell proliferation and migration rates in a computational model of sprouting angiogenesis,” *Sci. Rep.*, vol. 6, p. 36992, Nov. 2016, doi: 10.1038/srep36992.

[49] M. E. Fallon, R. Mathews, and M. T. Hinds, “In Vitro Flow Chamber Design for the Study of Endothelial Cell (Patho)Physiology,” *J. Biomech. Eng.*, vol. 144, no. 2, p. 020801, Feb. 2022, doi: 10.1115/1.4051765.

[50] M. Franzoni, I. Cattaneo, B. Ene-Iordache, A. Oldani, P. Righettini, and A. Remuzzi, “Design of a cone-and-plate device for controlled realistic shear stress stimulation on endothelial cell monolayers,” *Cytotechnology*, vol. 68, no. 5, pp. 1885–1896, Oct. 2016, doi: 10.1007/s10616-015-9941-2.

[51] H. Flohr and W. Breull, “Effect of etafenone on total and regional myocardial blood flow,” *Arzneimittelforschung.*, vol. 25, no. 9, pp. 1400–1403, Sep. 1975.

[52] H. Kim, K. Yang, and H. Cho, “Different Effects of Orbital Shear Stress on Vascular Endothelial Cells: Comparison with the Results of In Vivo Study with Rats,” *Vasc. Spec. Int.*, vol. 2, pp. 33–40, doi: https://doi.org/10.5758%2Fvsi.2015.31.2.33.

[53] A. Fernandes, V. Hosseini, V. Vogel, and R. D. Lovchik, “Engineering solutions for biological studies of flow-exposed endothelial cells on orbital shakers,” *PLOS ONE*, vol. 17, no. 1, p. e0262044, Jan. 2022, doi: 10.1371/journal.pone.0262044.

[54] X. Li and C.-Y. Wang, “From bulk, single-cell to spatial RNA sequencing,” *Int. J. Oral Sci.*, vol. 13, no. 1, p. 36, Dec. 2021, doi: 10.1038/s41368-021-00146-0.

[55] S. Aydin, “A short history, principles, and types of ELISA, and our laboratory experience with peptide/protein analyses using ELISA,” *Peptides*, vol. 72, pp. 4–15, Oct. 2015, doi: 10.1016/j.peptides.2015.04.012.

[56] A. V. Lin, “Indirect ELISA,” in *ELISA*, vol. 1318, R. Hnasko, Ed., in Methods in Molecular Biology, vol. 1318. , New York, NY: Springer New York, 2015, pp. 51–59. doi: 10.1007/978-1-4939-2742-5_5.

[57] X. Lu, X. Zhao, C. Bai, C. Zhao, G. Lu, and G. Xu, “LC–MS-based metabonomics analysis,” *J. Chromatogr. B*, vol. 866, no. 1–2, pp. 64–76, Apr. 2008, doi: 10.1016/j.jchromb.2007.10.022.

[58] E. Makareeva and S. Leikin, “Collagen Structure, Folding and Function,” in *Osteogenesis Imperfecta*, Elsevier, 2014, pp. 71–84. doi: 10.1016/B978-0-12-397165-4.00007-1.

[59] B. Burkel, B. A. Morris, S. M. Ponik, K. M. Riching, K. W. Eliceiri, and P. J. Keely, “Preparation of 3D Collagen Gels and Microchannels for the Study of 3D Interactions In Vivo,” *J. Vis. Exp. JoVE*, no. 111, p. 53989, May 2016, doi: 10.3791/53989.

[60] T. Ziegler, R. W. Alexander, and R. M. Nerem, “An endothelial cell-smooth muscle cell co-culture model for use in the investigation of flow effects on vascular biology,” *Ann. Biomed. Eng.*, vol. 23, no. 3, pp. 216–225, May 1995, doi: 10.1007/BF02584424.

[61] B. Good, “TOWARDS A FLUID-STRUCTURE INTERACTION MODEL OF THE PENN STATE PNEUMATIC PULSATILE PEDIATRIC VENTRICULAR ASSIST DEVICE.” The Pennsylvania State University, 2017. [Online]. Available: https://etda.libraries.psu.edu/files/final_submissions/14419

[62] D. G. Altman and J. M. Bland, “Standard deviations and standard errors,” *BMJ*, vol. 331, no. 7521, p. 903, Oct. 2005, doi: 10.1136/bmj.331.7521.903.

[63] A. Dardik *et al.*, “Differential effects of orbital and laminar shear stress on endothelial cells,” *J. Vasc. Surg.*, vol. 41, no. 5, pp. 869–880, May 2005, doi: 10.1016/j.jvs.2005.01.020.

[64] S. Dimmeler, I. Fleming, B. Fisslthaler, C. Hermann, R. Busse, and A. M. Zeiher, “Activation of nitric oxide synthase in endothelial cells by Akt-dependent phosphorylation,” *Nature*, vol. 399, no. 6736, pp. 601–605, Jun. 1999, doi: 10.1038/21224.

[65] J. A. Sotelo *et al.*, “Normal values of wall shear stress in the pulmonary artery from 4D flow data,” *J. Cardiovasc. Magn. Reson.*, vol. 14, no. S1, p. W66, Dec. 2012, doi: 10.1186/1532-429X-14-S1-W66.

[66] L. Zhang *et al.*, “Phospholipase Cε Hydrolyzes Perinuclear Phosphatidylinositol 4-Phosphate to Regulate Cardiac Hypertrophy,” *Cell*, vol. 153, no. 1, pp. 216–227, Mar. 2013, doi: 10.1016/j.cell.2013.02.047.

[67] P. Kikas, Democritus University of Thrace, Alexandroupolis, Greece, G. Chalikias, and Democritus University of Thrace, Alexandroupolis, Greece, “Cardiovascular Implications of Sphingomyelin Presence in Biological Membranes,” *Eur. Cardiol. Rev.*, vol. 13, no. 1, p. 42, 2018, doi: 10.15420/ecr.2017:20:3.

[68] E. Vianello *et al.*, “Circulating perturbation of phosphatidylcholine (PC) and phosphatidylethanolamine (PE) is associated to cardiac remodeling and NLRP3 inflammasome in cardiovascular patients with insulin resistance risk,” *Exp. Mol. Pathol.*, vol. 137, p. 104895, Jun. 2024, doi: 10.1016/j.yexmp.2024.104895.

[69] J. Liu *et al.*, “A multi-omics study of circulating phospholipid markers of blood pressure,” *Sci. Rep.*, vol. 12, no. 1, p. 574, Jan. 2022, doi: 10.1038/s41598-021-04446-7.

[70] A. Kvasnička *et al.*, “Long-chain polyunsaturated fatty acid-containing phosphatidylcholines predict survival rate in patients after heart failure,” *Heliyon*, vol. 10, no. 21, p. e39979, Nov. 2024, doi: 10.1016/j.heliyon.2024.e39979.

[71] A. Sigruener, M. E. Kleber, S. Heimerl, G. Liebisch, G. Schmitz, and W. Maerz, “Glycerophospholipid and Sphingolipid Species and Mortality: The Ludwigshafen Risk and Cardiovascular Health (LURIC) Study,” *PLoS ONE*, vol. 9, no. 1, p. e85724, Jan. 2014, doi: 10.1371/journal.pone.0085724.

[72] M. Wagner, B. Hampel, D. Bernhard, M. Hala, W. Zwerschke, and P. Jansen-Dürr, “Replicative senescence of human endothelial cells in vitro involves G1 arrest, polyploidization and senescence-associated apoptosis,” *Exp. Gerontol.*, vol. 36, no. 8, pp. 1327–1347, Aug. 2001, doi: 10.1016/S0531-5565(01)00105-X.

[73] M. Bennett, “Apoptosis of vascular smooth muscle cells in vascular remodelling and atherosclerotic plaque rupture,” *Cardiovasc. Res.*, vol. 41, no. 2, pp. 361–368, Feb. 1999, doi: 10.1016/S0008-6363(98)00212-0.

[74] B. S. Hays *et al.*, “Histopathological abnormalities in the central arteries and veins of Fontan subjects,” *Heart*, vol. 104, no. 4, pp. 324–331, Feb. 2018, doi: 10.1136/heartjnl-2017-311838.

[75] A. Krüger-Genge, A. Blocki, R.-P. Franke, and F. Jung, “Vascular Endothelial Cell Biology: An Update,” *Int. J. Mol. Sci.*, vol. 20, no. 18, p. 4411, Sep. 2019, doi: 10.3390/ijms20184411.

[76] “What are stress fibers?,” *Mechanobiol. Inst.*, [Online]. Available: https://www.mbi.nus.edu.sg/mbinfo/what-are-stress-fibers/

[77] J. M. Owen and K. J. Dormer, “The Shear Stress/KLF2/Nrf2/ARE Pathway: A Hemodynamic Defense against Oxidative Stress,” in *Blood - Updates on Hemodynamics and Thalassemia*, A. Seda Artis, Ed., IntechOpen, 2022. doi: 10.5772/intechopen.99566.

[78] F. Contijoch *et al.*, “Exercise MRI highlights heterogeneity in cardiovascular mechanics among patients with Fontan circulation: proposed protocol for routine evaluation,” *J. Thorac. Dis.*, vol. 12, no. 3, pp. 1204–1212, Mar. 2020, doi: 10.21037/jtd.2019.09.59.

[79] J. Singh *et al.*, “Patient-specific flow descriptors and normalised wall index in peripheral artery disease: a preliminary study,” *Comput. Methods Biomech. Biomed. Eng. Imaging Vis.*, vol. 6, no. 2, pp. 119–127, Mar. 2018, doi: 10.1080/21681163.2016.1184589.

[80] A. B. Fisher, S. Chien, A. I. Barakat, and R. M. Nerem, “Endothelial cellular response to altered shear stress,” *Am. J. Physiol.-Lung Cell. Mol. Physiol.*, vol. 281, no. 3, pp. L529–L533, Sep. 2001, doi: 10.1152/ajplung.2001.281.3.L529.

[81] Q. Gao *et al.*, “Mono- and Digalactosyldiacylglycerol Lipids Function Nonredundantly to Regulate Systemic Acquired Resistance in Plants,” *Cell Rep.*, vol. 9, no. 5, pp. 1681–1691, Dec. 2014, doi: 10.1016/j.celrep.2014.10.069.

[82] R. C. Murphy and P. H. Axelsen, “Mass spectrometric analysis of long-chain lipids,” *Mass Spectrom. Rev.*, vol. 30, no. 4, pp. 579–599, 2011, doi: 10.1002/mas.20284.

[83] D. B. Foster *et al.*, “The Cardiac Acetyl-Lysine Proteome,” *PLoS ONE*, vol. 8, no. 7, p. e67513, Jul. 2013, doi: 10.1371/journal.pone.0067513.

[84] F. Z. Mónica, K. Bian, and F. Murad, “The Endothelium-Dependent Nitric Oxide–cGMP Pathway,” in *Advances in Pharmacology*, vol. 77, Elsevier, 2016, pp. 1–27. doi: 10.1016/bs.apha.2016.05.001.

[85] S. O. E. Ebbesson *et al.*, "Fatty acids linked to cardiovascular mortality are associated with risk factors," *Int. J. Circumpolar Health*, vol. 74, no. 1, p. 28055, Jan. 2015, doi: 10.3402/ijch.v74.28055.

[86] S. K. Lahiri *et al.*, "Altered myocardial lipid regulation in junctophilin-2–associated familial cardiomyopathies," *Life Sci. Alliance*, vol. 7, no. 5, p. e202302330, May 2024, doi: 10.26508/lsa.202302330.

[87] N. Jin *et al.*, "Identification of potential serum biomarkers for congenital heart disease children with pulmonary arterial hypertension by metabonomics," *BMC Cardiovasc. Disord.*, vol. 23, no. 1, p. 167, Mar. 2023, doi: 10.1186/s12872-023-03171-5.

[88] R. Johnson Kameny *et al.*, "Ovine Models of Congenital Heart Disease and the Consequences of Hemodynamic Alterations for Pulmonary Artery Remodeling," *Am. J. Respir. Cell Mol. Biol.*, vol. 60, no. 5, pp. 503–514, May 2019, doi: 10.1165/rcmb.2018-0305MA.

[89] A. Karlstaedt, X. Zhang, H. Vasquez, M. A. Goodell, and H. Taegtmeyer, "Abstract 385: D-2-hydroxyglutaric acid Acutely Impairs Oxidative Decarboxylation in the Heart," *Circ. Res.*, vol. 117, no. suppl_1, Jul. 2015, doi: 10.1161/res.117.suppl_1.385.

[90] R. T. Ribeiro *et al.*, "Disruption of mitochondrial bioenergetics, calcium retention capacity and cell viability caused by D-2-hydroxyglutaric acid in the heart," *Biochimie*, vol. 207, pp. 153–164, Apr. 2023, doi: 10.1016/j.biochi.2022.11.004.

[91] H. Li and A. B. Hummon, "Imaging Mass Spectrometry of Three-Dimensional Cell Culture Systems," *Anal. Chem.*, vol. 83, no. 22, pp. 8794–8801, Nov. 2011, doi: 10.1021/ac202356g.

[92] K. Sato, M. Nakajima, S. Tokuda, and A. Ogawa, "Fluidic Culture and Analysis of Pulmonary Artery Smooth Muscle Cells for the Study of Pulmonary Hypertension," *Anal. Sci.*, vol. 32, no. 11, pp. 1217–1221, Nov. 2016, doi: 10.2116/analsci.32.1217.

[93] A. L. Cheng, N. M. Pahlevan, D. G. Rinderknecht, J. C. Wood, and M. Gharib, "Experimental investigation of the effect of non-Newtonian behavior of blood flow in the Fontan circulation," *Eur. J. Mech. - BFluids*, vol. 68, pp. 184–192, Mar. 2018, doi: 10.1016/j.euromechflu.2017.12.009.

APPENDIX

Cell Culture Protocols

Maintaining a Sterile Environment

Wash hands and wear proper protective equipment prior to touching the cells. PPE includes a lab coat, gloves, booties, goggles, mask, and tying back of long hair. Change gloves after touching any items outside of the biosafety cabinet. Do not let coat sleeves touch the inner surface of the biosafety cabinet. Do not touch pipet tips with hands or let them touch any other surface besides the fluid being pipetted. Always change pipet tips before collecting stock fluids to avoid cross contamination. Reduce the amount of time that bottles and flasks are opened by keeping caps on until use. Change water bath water frequently, and do not let bottles flip over in the bath. Always use autoclaved water. Clean frequently.

Thawing Cells

When thawing from stock, follow supplier information and procedures. To thaw from cryopreserved lab cells, open the dewar and remove the vials of which are to be thawed. Hold the vial in a water bath to quickly thaw the cells, be sure to not submerge the cap. Pipet the cell and cryopreservation media from the cryovial and deposit into a fresh cell flask with new media. Label the cell flask with the date, type of cells, type of media, and the passage. Change the media the day after to allow the cells to adhere to the flask.

Making Media

In order to make new media, thaw out all necessary media components, spray with alcohol and place in the biosafety cabinet. Use a vacuum and filter system to filter the media components and mix them thoroughly. Label the new bottle with media components and the date.

Media Change

For a media change, warm cell media from the making media procedure and spray with alcohol and add to biosafety cabinet. Place cell flasks that need a media change in the biosafety cabinet. Remove used media and deposit in a bleach bucket with a pipet. Add the necessary amount of new media back to the flask. Cell media should be changed every 2-3 days.

Splitting Cells

Cell splitting should be done when cells reach 70-90% confluency. To split cells, begin by following the media change procedure until the removal of used media step. Add 5 mL of saline to cell flask and swirl, then remove and deposit to bleach bucket. Repeat twice. Add 5 mL

of trypsin EDTA to cell flask, and incubate for 5-10 minutes; cell adhesion levels can be monitored by observing on the microscope. Once cells have detached, add double the amount of cell media and aspirate in the cell flask to neutralize the trypsin EDTA. Remove mixture and add to a tube with labeled information. Place in the centrifuge at 1640 RPM for 5 minutes. A thin white layer of cells should form in the bottom of the tube. Dispose of mixture into the bleach bucket without disturbing the cell pellet. Resuspend the cells in fresh media and count the cells with a cell counter. Add to the necessary amount of new cell flasks and label with date, cell type, media type, and passage.

Freezing Cells

To freeze cells, proceed by following the splitting cells procedure until the post centrifuge resuspension step. After dumping remaining media post centrifuge, resuspend the cells in an approved cryopreservation media. Aspirate the cells while maintaining a constant speed and count the cells with the cell counter. Make note of the number of cells being frozen, then deposit the cryopreservation media and cell mixture into cryovials accordingly. Label each cryovial with the date, type of cells, and passage number. Place cryovials into a slow freezing capsule, and then place it into a -80 freezer. After at least 24 hours, remove the capsule, remove the vials, and place the vials in a liquid nitrogen dewar.

Cell Contamination

Contamination can happen at any time, from mostly any cause. There are three main types of contamination- bacteria, viruses, and yeast. Signs of contamination may include the media changing colors, cloudy media, or observation of other particles besides cells on the microscope. Antibiotics can be used to clear bacterial contamination.

Autoclaving

Fill glass bottles with water and slightly screw the caps back on. Do not tighten them-screw as to only keep them from falling off the bottle. Place a strip of autoclave tape over the cap to keep it from boiling off in the autoclave. Place bottles with water in a secondary, autoclave safe container. Use a cart to transfer bottles to autoclave. Place the secondary container with bottles into the autoclave. Close the autoclave door and turn the lock to slightly past hand tight. Refer to local protocols for exact parameters. Begin a cycle, and once completed return to the autoclave. Remove secondary container and bottles with great caution to avoid hot water burns. Use autoclave gloves and PPE.

Liquid Nitrogen Handling

Be sure to wear proper PPE, including cryo gloves. Roll dewar to liquid nitrogen tank, remove insulated lid, and insert nitrogen tube into dewar. Ensure that the tube is in the hole in the bottom of the dewar. Turn on liquid nitrogen, and fill dewar to approximately 9 inches.

Protocols

Nitric Oxide ELISA

Sigma-Aldrich.

SigmaAldrich.com

Technical Bulletin

Nitric Oxide Assay Kit

Catalog Number MAK454

Product Description

Nitric oxide (NO) is a reactive radical that plays an important role in many key physiological functions. NO, an oxidation product of arginine by nitric oxide synthase, is involved in host defense and development, activation of regulatory proteins and direct covalent interaction with functional biomolecules.

Simple, direct and automation-suitable procedures for measuring NO are valuable in research and drug discovery. Since NO is oxidized to nitrite and nitrate, it is common practice to quantitate total NO_2^-/NO_3^- as a measure for NO level. The Nitric Oxide Assay Kit is designed to accurately measure NO production following reduction of nitrate (NO_3^-) to nitrite (NO_2^-) using an improved Griess method. The procedure is simple, and the time required for sample pretreatment and assay is to as short as 30 minutes. The detection range of the assay method is 0.6 – 100 µM.

The kit is suitable for the quantitative determination of nitric oxide (nitrate/nitrite) and evaluation of drug effects on its metabolism in plasma, serum, urine, tissue, cells and foods.

Components

The kit is sufficient for 100 colorimetric assays in 96-well plates.

- Reagent A — 12 mL
  Catalog Number MAK454A
- Reagent B — 500 µL
  Catalog Number MAK454B
- Reagent C — 12 mL
  Catalog Number MAK454C
- NaOH — 1 mL
  Catalog Number MAK454D
- $ZnSO_4$ — 1 mL
  Catalog Number MAK454E
- Standard (1.0 mM) — 1 mL
  Catalog Number MAK454F

Reagents and Equipment Required but Not Provided

- Pipetting devices and accessories (e.g., multichannel pipettor)
- Spectrophotometric multiwell plate reader
- Clear flat-bottom 96-well plates. Cell culture or tissue culture treated plates are **not** recommended.
- Refrigerated microcentrifuge capable of RCF ≥ 14,000 × *g*
- 1.5 mL microcentrifuge tubes
- Phosphate Buffered Saline (PBS) (Catalog Number P3813 or equivalent)

MilliporeSigma

Precautions and Disclaimer

For R&D use only. Not for drug, household, or other uses. Please consult the Safety Data Sheet for information regarding hazards and safe handling practices.

Storage/Stability

The kit is shipped on wet ice. Store components at -20 °C.

Preparation Instructions

Briefly centrifuge small vials prior to opening. Prior to use, equilibrate all components to room temperature.

Reagent B: If precipitates are present, warm for ~10-15 minutes at 37 °C until redissolved.

Procedure

All samples and standards should be run in duplicate.

Sample Preparation

Note: Antioxidants and nucleophiles (e.g., β-mercaptoethanol, glutathione, dithiothreitol and cysteine) may interfere with this assay. Avoid using these compounds during sample preparation.

Tissue and Cells

Homogenize tissue or cell samples in 1× PBS (pH 7.4). Note: The amount of tissue or cells used varies and depends heavily on the nitrate/nitrite content. It is recommended to run a pilot study to determine the proper tissue/cell to PBS volume ratio. Centrifuge at 14,000 × g at 4 °C. Retain supernatant for use in NO assay.

Deproteination

Samples that need deproteination include serum, plasma, whole blood, cell culture media containing FBS, tissue and cell lysates. Urine and saliva do not need deproteination.

1. Mix 150 µL of Sample with 8 µL of $ZnSO_4$ in 1.5 mL tubes.
2. Vortex and then add 8 µL NaOH.
3. Vortex again and centrifuge for 10 minutes at 14,000 × *g*.
4. Transfer 100 µL of the clear supernatant to separate, labeled 1.5 mL microcentrifuge tubes. Samples should be performed in duplicate at a minimum.

Standard Curve Preparation

Note: If Sample Deproteination was required, prepare a 150 µL aliquot of each Standard and treat with $ZnSO_4$ and NaOH as described under Deproteination section to eliminate the need for a dilution factor.

1. Prepare a 100 µM Nitrite Standard by mixing 50 µL of the 1.0 mM Standard with 450 µL of purified water.
2. Prepare Nitrite Standards in 1.5 mL microcentrifuge tubes according to Table 1.

Table 1.
Preparation of Nitrite Standards

Well	100 µM Nitrite Standard	Purified Water	Nitrite (µM)
1	250 µL	-	100
2	150 µL	100 µL	60
3	75 µL	175 µL	30
4	-	250 µL	0

3. Mix well and transfer 100 µL of each Standard to separate, labeled 1.5 mL microcentrifuge tubes.

Working Reagent

Immediately prior to starting the reaction, mix enough Working Reagent for the number of assays to be performed. For each Sample and Standard, prepare 204 µL of Working Reagent according to Table 2.

Table 2.
Preparation of Working Reagent

Reagent	Working Reagent
Reagent A	100 µL
Reagent B	4 µL
Reagent C	100 µL

Assay Reaction

1. Add 200 µL of Working Reagent to each Sample and Standard tube.
2. Mix well and incubate for 10 minutes at 60 °C. Alternatively, the reaction can be run at 37 °C for 60 minutes or at room temperature for 150 minutes.

Measurement

1. Briefly centrifuge the reaction tubes to pellet any condensation.
2. Transfer 250 µL of each reaction solution to separate wells of a clear 96-well plate.
3. Read optical density (OD) at 540 nm.

Results

1. Subtract the blank OD (Standard #4) value from the remaining Standard OD values.
2. Plot the corrected Standard OD values against the Standard concentrations and determine the slope of the Standard curve.
3. Calculate the Nitric Oxide concentration of Sample:

Nitric Oxide (µM) =

$$\frac{OD_{Sample} - OD_{Blank}}{Slope} \times DF$$

where

OD_{Sample} = Optical density (OD) reading of the Sample

OD_{Blank} = Optical density (OD) reading of the Blank (Standard #4)

DF = Sample Dilution factor (DF = 1 for undiluted Samples)

Note: If the calculated nitric oxide concentration of the Sample is higher than 100 µM, dilute the Sample in purified water and repeat the assay.

Conversions: 1 mg/dL NO equals 333 µM, 0.001% or 10 ppm.

Figure 1.
Typical Nitric Oxid Standard Curve

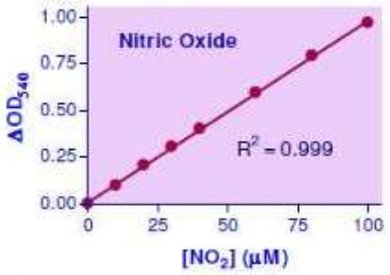

References

1. Kim, H.-C., et al., Cobalt(II)-coordination polymers containing glutarates and bipyridyl ligands and their antifungal potential. *Sci. Rep.*, **9(1)** (2019), DOI: 10.1038/s41598-019-50258-1.
2. Kang, M., et al., Plasma mediated disinfection of rice seeds in water and air. *J. Phys. D: Appl. Phys*, **53**, 214001 (2020).
3. Veerana, M., et al., Analysis of the effects of Cu-MOFs on fungal cell inactivation. *RSC Adv.*, **11**, 1057-1065 (2021).

Notice

We provide information and advice to our customers on application technologies and regulatory matters to the best of our knowledge and ability, but without obligation or liability. Existing laws and regulations are to be observed in all cases by our customers. This also applies in respect to any rights of third parties. Our information and advice do not relieve our customers of their own responsibility for checking the suitability of our products for the envisaged purpose.

The information in this document is subject to change without notice and should not be construed as a commitment by the manufacturing or selling entity, or an affiliate. We assume no responsibility for any errors that may appear in this document.

Contact Information

For the location of the office nearest you, go to SigmaAldrich.com/offices.

Technical Service

Visit the tech service page on our web site at SigmaAldrich.com/techservice.

Standard Warranty

The applicable warranty for the products listed in this publication may be found at SigmaAldrich.com/terms.

VEGF ELISA

Millipore

www.sigmaaldrich.com

Certificate of Analysis / Protocol

3050 Spruce Street, Saint Louis, MO 63103 USA
Tel: (800) 521-8956 (314) 771-5765 Fax: (800) 325-5052
(314) 771-5757

Product Name	Mouse VEGF ELISA Kit for cell and tissue lysates
Product Number	RAB0510
Lot Number	0131K0435
Storage	Store the kit at -20°C. It remains active for up to 1 year. Avoid repeated freeze-thaw cycles. The reconstituted standard should be stored at -20°C or -70°C (-70°C is recommended). Opened microplate strips or reagents may be store for up to 1 month at 2-8°C. Return unused wells to the pouch containing desiccant pack and reseal along entire edge.
Components	1. Mouse VEGF Antibody-coated ELISA Plate (Item A) - RABMVEGFA-EA: 96 wells (12 strips x 8 wells) coated with anti-Mouse VEGF. 2. 20x Wash Buffer (Item B) - RABWASH4 3. Lyophilized Mouse VEGF Protein Standard (Item C) - RABVEGFFS-1VL 4. Biotinylated Mouse VEGF Detection Antibody (Item F) - RABMVEGFF-1VL 5. HRP-Streptavidin (Item G) - RABHRP5 6. ELISA Colorimetric TMB Reagent (HRP Substrate, Item H) - RABTMB3 7. ELISA Stop Solution (Item I) - RABSTOP3 8. ELISA 5x Sample Diluent Buffer (Item D2) - RABDIL6-10ML 9. ELISA 5x Assay/Sample Diluent Buffer (Item E2) - RABELADE-15ML 10. 2X Cell Lysis Buffer (Item J) - RABLYSIS1-5ML
Assay/Sample Diluent Buffer dilution (Preparation, Step 2)	Sample Diluent Buffer (Item D2) and Assay/Sample Diluent Buffer (Item E2) should be diluted 5-fold with deionized or distilled water before use. Cell lysis buffer (Item J) should be diluted 2-fold with deionized or distilled water (for cell lysate and tissue lysate).

Sample Dilution (Preparation, Step 3)

Tissue lysate and cell lysate samples should be diluted at least 5-fold with 1X Sample Diluent Buffer (Item D2). Generally we recommend a minimum of 1 mg of protein per 1 ml of original lysate solution, though more concentrated is better. We also recommend the addition of protease inhibitors (not included) to the lysis buffer prior to use.

* Please note that the levels of VEGF may vary between different samples. Optimal dilution factors for each sample must be determined by the investigator.

Preparation of Standard (Preparation, Step 4)

Briefly spin a vial of Item C. Add 400 µl 1X Sample Diluent Buffer (Item D2) into Item C vial to prepare a 25 ng/ml standard. Dissolve the powder thoroughly by a gentle mix. Add 40 µl VEGF standard from the vial of Item C, into a tube with 960.0 µl Sample Diluent Buffer to prepare a 1,000 pg/ml stock standard solution. Pipette 300 µl 1X Sample Diluent Buffer into each tube. Use the stock standard solution to produce a dilution series (Figure 1). Mix each tube thoroughly before the next transfer. 1X Sample Diluent Buffer serves as the zero standard (0 pg/ml).

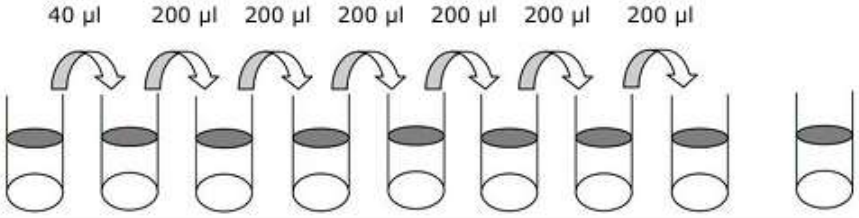

		Std1	Std2	Std3	Std4	Std5	Std6	Std7		Zero Standard
Diluent volume	Item C+ 400 µl	960 µl	300 µl	300 µl	300 µl	300 µl	300 µl	300 µl		300 µl
Conc.	25 ng/ml	1000 pg/ml	400 pg/ml	160 pg/ml	64 pg/ml	25.6 pg/ml	10.2 pg/ml	4.1 pg/ml		0 pg/ml

Preparation of Biotinylated Detection Antibody (Preparation, Step 6)

Briefly spin the Detection Antibody vial (Item F) before use. Add 100 µl of 1x Diluent Buffer (Item E2) into the vial to prepare a detection antibody concentrate. Pipette up and down to mix gently (the concentrate can be stored at 4°C for 5 days). The detection antibody concentrate should be diluted 80-fold with 1x Diluent Buffer (Item E2) and used in Procedure, step 4.

Dilution of HRP-Streptavidin Concentrate (Preparation, Step 7)

Briefly spin the HRP-Streptavidin concentrate vial (Item G) and pipette up and down to mix gently before use, as precipitates may form during storage. HRP-Streptavidin concentrate should be diluted 160-fold with 1x Diluent Buffer (Item E2).
For example: Briefly spin the vial (Item G) and pipette up and down to mix gently. Add 100 µl of HRP-Streptavidin concentrate into a tube with 16 ml 1X Assay Diluent to prepare a 160-fold diluted HRP-Streptavidin solution (don't store the diluted solution for next day use). Mix well.

Sandwich Assay Procedure

1. Bring all reagents and samples to room temperature (18 - 25°C) before use. It is recommended that all standards and samples be run at least in duplicate.
2. Add 100 µl of each standard and sample into appropriate wells. Cover wells and incubate for 2.5 hours at room temperature or overnight at 4°C with gentle shaking.
3. Discard the solution and wash 4 times with 1X Wash Solution. Wash by filling each well with Wash Buffer (300 µl) using a multi-channel Pipette or autowasher. Complete removal of liquid at each step is essential to good performance. After the last wash, remove any remaining Wash Buffer by aspirating or decanting. Invert the plate and blot it against clean paper towels.
4. Add 100 µl of 1x prepared Detection Antibody to each well. Cover wells and incubate for 1 hour at room temperature with gentle shaking.
5. Discard the solution. Repeat the wash procedure as in step 3.
6. Add 100 µl of prepared Streptavidin solution to each well. Cover wells and incubate for 45 minutes at room temperature with gentle shaking.
7. Discard the solution. Repeat the wash as in step 3.
8. Add 100 µl of TMB One-Step Substrate Reagent (Item H) to each well. Cover wells and incubate for 30 minutes at room temperature in the dark with gentle shaking.
9. Add 50 µl of Stop Solution (Item I) to each well. Read absorbance at 450 nm immediately.

Fig 2: Example of the Sandwich ELISA process

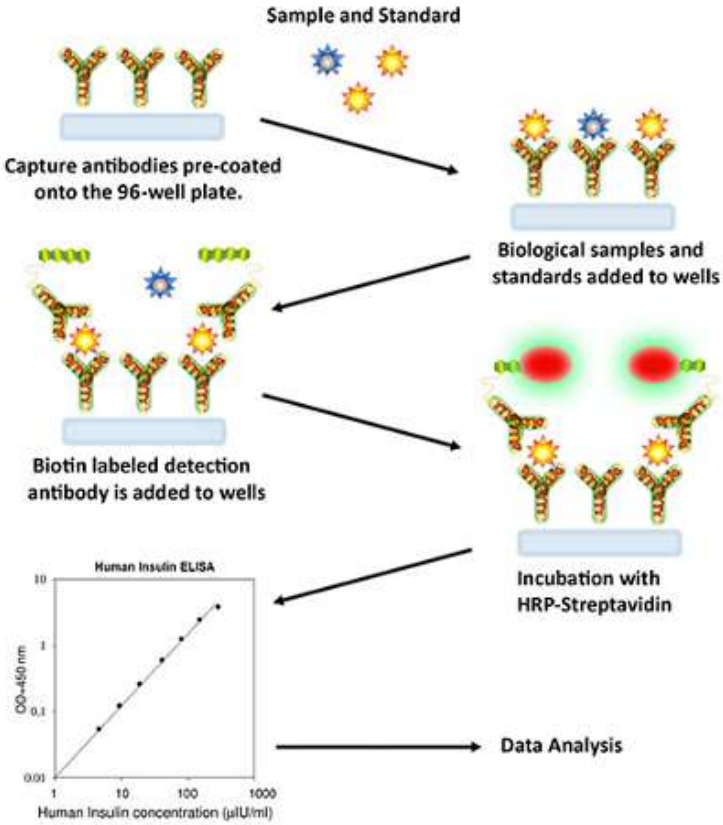
Sample and Standard
Capture antibodies pre-coated onto the 96-well plate.
Biological samples and standards added to wells
Biotin labeled detection antibody is added to wells
Incubation with HRP-Streptavidin
Human Insulin ELISA
OD-450 nm
10
1
0.1
0.01
1
10
100
1000
Human Insulin concentration (µIU/ml)
Data Analysis

Typical Data

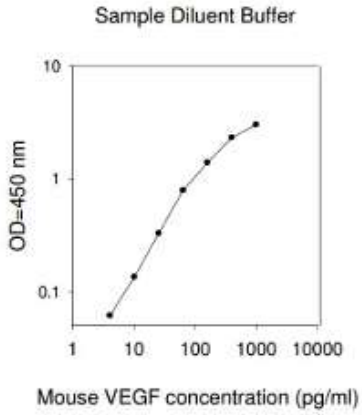

Sensitivity

The minimum detectable dose of Mouse VEGF was determined to be 2 pg/ml.

Minimum detectable dose is defined as the analyte concentration resulting in an absorbance that is 2 standard deviations higher than that of the blank (diluent buffer).

Recovery

Recovery was determined by spiking various levels of Mouse VEGF into the sample types listed below. Mean recoveries are as follows:

Sample Type	Average % Recovery	Range (%)
Tissue lysate	87.87	81-102
Cell lysate	88.62	82-103

LINEARITY

Sample Type		Tissue Lysate	Cell lysate
1:2	Average % of Expected Range (%)	92 82-102	93 83-103
1:4	Average % of Expected Range (%)	95 84-103	96 85-105

Intra-Assay Reproducibility	CV < 10%
Inter-Assay Reproducibility	CV < 12%
Specificity	The antibody pair provided in this kit recognizes mouse VEGF.

This certificate is system generated and does not require a signature

Product of USA, MSDS available
For research use only. Not for use in diagnostic procedures.

Sigma-Aldrich, Inc. warrants that its products conform to the information contained in this and other Sigma-Aldrich Publications. Purchaser must determine the suitability of the product(s) for their particular use.

Additional terms and conditions may apply. Please see reverse side of the invoice or packing slip

Collagen Gel

upstate | CHEMICON | Linco
THE EXPERTISE OF UPSTATE®, CHEMICON® AND LINCO® IS NOW A PART OF MILLIPORE

Certificate of Analysis

Collagen, Type I, Rat Tail

(Extracted from rat tail tendons)

Catalog # 08-115

Lot # 4061395

Source: Rat tendon excised from tail.

Physical Form: Liquid (Slight turbidity may be observed. Turbidity does not affect product functionality).

Formulation: 100 mg in 30.8 mL 0.02N acetic acid.

Concentration: 3.25 mg/mL.

Storage and Stability: Stable for 1 year at 4°C from date of shipment. DO NOT FREEZE**.**

FOR RESEARCH USE ONLY; NOT FOR USE IN DIAGNOSTIC PROCEDURES. NOT FOR HUMAN OR ANIMAL CONSUMPTION

Quality Control Testing

Cell Adhesion Assay: This lot of collagen has been tested for tested for uniform gelation and for attachment of spreading of PC-12 rat cells.

Endotoxin: This lot of collagen has been tested for and endotoxin levels, and is < 1 EU/µg.

Mycoplasma Testing: This lot of collagen has been tested and found negative for the presence of mycoplasma.

Coating Procedures

Firm Collagen Gel

Pipette 0.25-0.3 mL of undiluted collagen into 35mm culture dishes and spread evenly.

Place the culture dishes in ammonia vapor chamber for 2-4 minutes (use ammonium hydroxide and saturate a sterile cotton ball in a closed container).

Remove cotton and add 5 mL of sterile, distilled water to the culture dishes, allow to stand for 1 hour and aspirate.

Repeat the previous step 3 four times to rid the substrate of ammonia.

Leave the last rinse in dish and hold overnight at 4°C.

Aspirate the final rinse and replace with sterile medium or balanced salt solution with 1-2% serum. Store at 4°C until use.

EMD Millipore Corporation, 28820 Single Oak Drive, Temecula, CA 92590, USA 1-800-437-7500

Technical Support: T: 1-800-MILLIPORE (1-800-645-5476) • F: 1-800-437-7502

www.millipore.com 08-115/05-MAR-2014/RevC/NJA

Catalog # 08-115

Lot # 4061395

Collagen Coating using PBS

Dilute collagen solution with PBS to 5-10 µg/cm^2.

Add diluted collagen to cover the surface.

Incubate at room temperature for 10-30 minutes and aspirate.

Wash with PBS or medium (washing is not always necessary).

Collagen Coating using EtOH

Dilute collagen solution with 30% Ethanol to 2.5 µg/cm^2.

Add diluted collagen to cover the surface.

Allow the Ethanol to evaporate under sterile conditions.

Cover and store at 4°C.

Unless otherwise stated in our catalog or other company documentation accompanying the product(s), our products are intended for research use only and are not to be used for any other purpose, which includes but is not limited to, unauthorized commercial uses, in vitro diagnostic uses, ex vivo or in vivo therapeutic uses or any type of consumption or application to humans or animals.

EMD Millipore Corporation, 28820 Single Oak Drive, Temecula, CA 92590, USA 1-800-437-7500

Technical Support: T: 1-800-MILLIPORE (1-800-645-5476) • F: 1-800-437-7502

www.millipore.com

Cell Culture Certificate of Analysis

Certificate of Analysis

Human Pulmonary Artery Endothelial Cells (HPAEC)

PromoCell

Description

Product Name	HPAEC-c / HPAEC-p
Order Number	C-12241 / C-12242
Lot Number	5012019.10
Donor Age / Sex / Ethnicity	76 / male / caucasian
Tissue / Localisation	pulmonary artery / main branch
Number of Viable Cells	650.000
Freezing Medium	Cryo-SFM (Order No.: C-29910)
QC Evaluation Medium	Endothelial Cell Growth Medium (Order No.: C-22010)
Stage of Culture	HPAEC-c: thawing and seeding results in passage 2 (3rd culture) HPAEC-p: shipped in passage 2 (3rd culture)

Viability & Growth Characteristics

Parameter	Test Method*	Result
Viability	Automated Viability Test	80 %
Population Doubling (PD) Time in Log Phase	Growth Promotion Test	27.5 h / PD
Population Doublings	Growth Promotion Test	>15 PD*

Phenotypic Characterization (tested within the first two passages)

Parameter	Test Method*	Result
CD31	Flow Cytometry	positive
Ac-LDL uptake	Flow Cytometry	positive

Test for microbiological contaminants and infectious viruses

Parameter	Test Method	Result
Bacteria, Fungi	Sterility Test	negative
Mycoplasma Genus, M. Pulmonis	PCR	negative
HIV-1, HIV-2	PCR	negative
HBV, HCV	PCR	negative
HTLV-1, HTLV-2	PCR	negative

* Using PromoCell's standardized culture system and procedures. The stated values may vary under customer culture conditions.

The tissue used by PromoCell for the isolation of human cell cultures is derived from donors who have signed an informed consent form, which outlines in detail the purpose of the donation and the procedure for processing the tissue (www.promocell.com/ethics).

Dr. Sabine Häcker
Head of Quality Control

Date: Dec 01, 2023

FOR IN VITRO RESEARCH USE ONLY. NOT FOR DIAGNOSTIC OR THERAPEUTIC PROCEDURES.

PromoCell GmbH
Sickingenstr. 63 / 65
69126 Heidelberg
Germany

North America
Deutschland
France
United Kingdom
Other Countries

1 – 866 – 251 – 2860 (toll free)
0800 – 776 66 25 (gebührenfrei)
0800 90 93 32 (ligne verte)
0800 – 96 03 33 (toll free)
+49 6221 – 649 34 0

Email: info@promocell.com
www.promocell.com

06/2022

VITA

Toni M. Perkins was born in Roanoke, Virginia. She attended Cave Spring High School and graduated with an advanced studies diploma. During her time there, she shadowed orthopedic surgeons at Carilion Memorial Hospital and participated in multiple clubs and sports. Toni attended the University of Tennessee, Knoxville, and earned a Bachelor of Science in Biomedical Engineering. She completed undergraduate research in Dr. Colleen Crouch's Lab, and an internship at Fresenius Medical Care North America. Her extracurricular activities during her undergraduate studies consisted of mentoring students through engineering organizations and initiating the founding of the sorority Alpha Sigma Kappa for women in technical studies. She also worked part time at Outdoor Gear Revival, participated in the Student Outdoor Leadership Experience, and earned her Wilderness First Aid Certification. Her education continued to a Master of Science in Biomedical Engineering at the University of Tennessee, Knoxville. Once again, she completed research in Dr. Crouch's Lab, this time as a graduate student. In addition, she served as a Graduate Teaching Assistant and Graduate Research Assistant during this time. Toni wrote her thesis "Response of Pulmonary Artery Endothelial Cells to Altered Stress Conditions" and later graduated in May 2025.